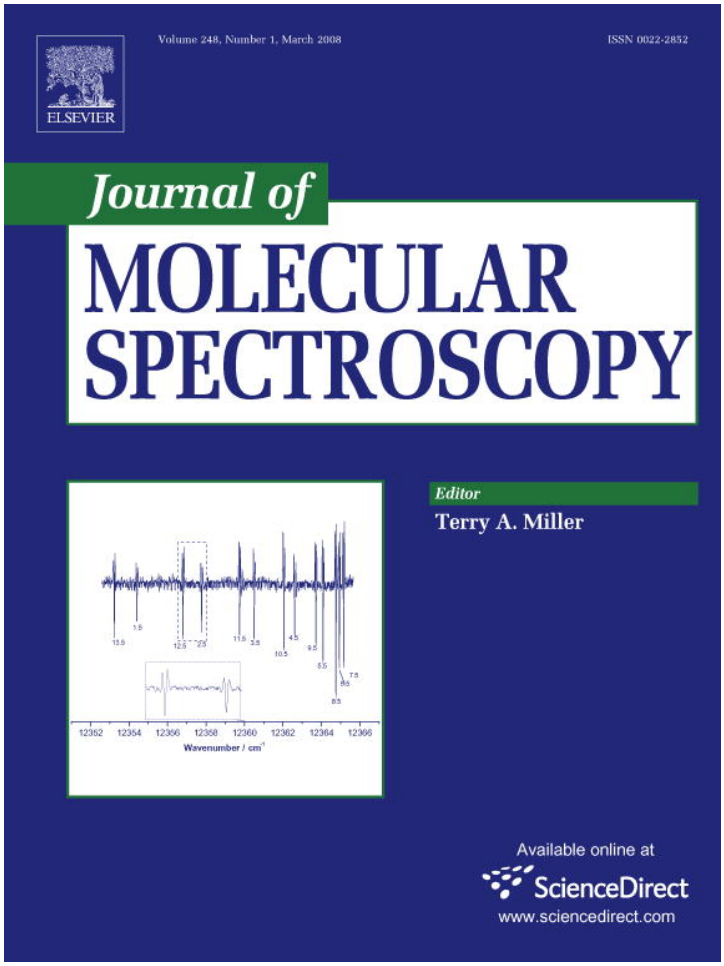

Available online at www.sciencedirect.com
ScienceDirect
Journal of Molecular Spectroscopy 248 (2008) 41–60
Journal of MOLECULAR SPECTROSCOPY
www.elsevier.com/locate/jms

Fourier-transform spectroscopy of $^{14}N^{15}N^{16}O$ in the 3800–9000 cm^{-1} region and global modeling of its absorption spectrum

H.-Y. Ni [a], K.-F. Song [a], V.I. Perevalov [b], S.A. Tashkun [b], A.-W. Liu [a], L. Wang [a], S.-M. Hu [a,*]

[a] *Department of Chemical Physics, Hefei National Laboratory for Physical Sciences at Microscale, University of Science and Technology of China, No. 96, Jin Zhai Lu Road, Hefei, Anhui 230026, China*

[b] *Laboratory of Theoretical Spectroscopy, Institute of Atmospheric Optics, Siberian Branch, Russian Academy of Sciences, Akademicheskii av. 1, 634055 Tomsk, Russia*

Received 4 November 2007; in revised form 20 November 2007
Available online 5 December 2007

Abstract

The absorption spectrum of $^{14}N^{15}N^{16}O$-enriched sample of nitrous oxide has been recorded at Doppler limited resolution with a Fourier-transform spectrometer in the spectral range 3500–9000 cm^{-1}. More than 12000 transitions of $^{14}N^{15}N^{16}O$ were observed and ro-vibrationally assigned on the basis of the global effective Hamiltonian model. The band-by-band analysis led to the determination of the ro-vibrational parameters of a total of 107 bands. Among the 107 bands, 80 are newly observed, for 27 others the rotational analysis is significantly extended and improved. The effective Hamiltonian parameters are determined from global fitting to the observed line positions presented in this paper and collected from the literature. As a result, a set of 117 obtained effective Hamiltonian parameters reproduces 16134 observed line positions of 148 bands with RMS of 0.0014 cm^{-1}.

Keywords: Nitrous oxide; Infrared; Fourier-transform spectroscopy; Line position; Spectroscopic parameters; Global model

1. Introduction

Nitrous oxide is a minor constituent of the Earth atmosphere. But as a greenhouse gas it plays an important role in the atmospheric radiation balance. This molecule also contributes very much to the ozone layer depletion. In addition, nitrous oxide is one of the burning products of the organic fuels in the air. As a consequence, the high-resolution spectra of this molecule are widely used for the monitoring of its concentration in atmosphere and in the combustion exhaust. $^{15}N^{14}N^{16}O$ and $^{14}N^{15}N^{16}O$ (natural abundance: 0.36409%) are the next two most abundant isotopic species of nitrous oxide after the principle isotopoloque $^{14}N^{15}N^{16}O$. In the last few decades, spectroscopic studies of the $^{14}N^{15}N^{16}O$ molecule have been carried out with microwave spectrometers (MW) [1–3], Fourier-transform infrared spectrometers (FTS) [4–10], intra-cavity laser absorption spectrometer (ICLAS) [11], and cavity ring-down spectrometer (CRDS) [12,13]. All the above listed measurements were carried out with natural nitrous oxide samples. Despite of all these publications, the high resolution spectra of $^{14}N^{15}N^{16}O$ in the near-IR region is still rather scarce. In present work, we focus on the line positions study of the $^{14}N^{15}N^{16}O$ isotopic species in the 3500–9000 cm^{-1} region. The study on the line intensities and transition dipole moments will be discussed later in a separate work. The knowledge of the $^{14}N^{15}N^{16}O$ spectra in the studied region will lead to better global modeling of its high-resolution spectra.

In Section 2, we present briefly the experimental conditions employed for the recording of the spectra. In Section 3, it is presented the ro-vibrational analysis of the recorded

* Corresponding author. Fax: +86 551 360 2969.
E-mail address: smhu@ustc.edu.cn (S.-M. Hu).

0022-2852/$ - see front matter © 2007 Elsevier Inc. All rights reserved.
doi:10.1016/j.jms.2007.11.011

spectra which includes the vibrational assignments and band-by-band rotational analysis. In Section 4, the local resonance perturbations observed in the investigated spectra are discussed.

2. Experimental details

The sample of nitrous oxide isotope $^{14}N^{15}N^{16}O$ was purchased from Icon Services Inc. The stated isotopic concentration is 99%. The accurate isotopic concentration was derived by a photo-ionization mass spectroscopy (PIMS) experiment, which was performed with a time-of-flight mass spectrometer in the photochemistry end-station of National Synchrotron Radiation Laboratory, Hefei. PIMS measurement has given the abundance of $^{14}N^{15}N^{16}O$ in the sample as 97.4% with about 0.2% accuracy. The absorption spectrum was recorded by a Bruker IFS 120HR interferometer with a path length adjustable multi-path gas cell. The whole interference chamber is vacuumed to less than 0.4 mBar to eliminate the atmospheric absorption. Because of the wide spectral range and the large variation of the absorption band intensities, different experimental conditions were applied in the measurements as listed in Table 1. The gas sample pressure was measured using two capacitance manometers (MKS Baratron 627B) of 1 and 20 Torr full-scale ranges with accuracy of 0.15%. In most measurements, varied optical filters were applied to improve the signal-to-noise ratio and allow high-resolution measurements. The lines of water vapor what appeared as minor contamination in the cell were adopted as reference lines for calibration. Their values were taken from the work of Toth [14]. The accuracy of the unblended and not-very-weak lines is estimated to be better than 0.001 cm^{-1}. An overview of the recorded spectrum is presented in Fig. 1.

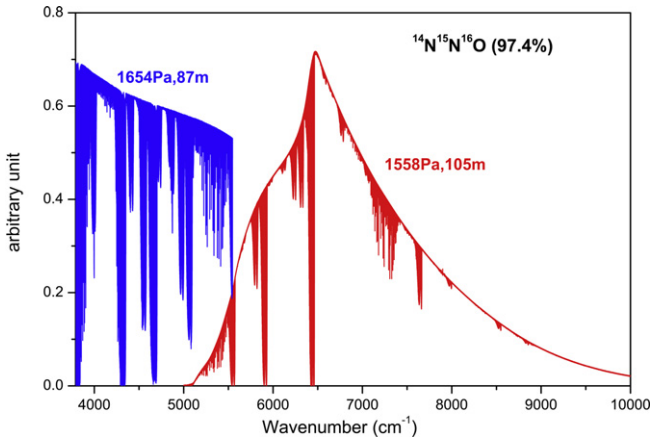

Fig. 1. The Fourier-transform absorption spectrum of $^{14}N^{15}N^{16}O$ in the region 3800–10000 cm^{-1}.

3. Rovibrational analysis

3.1. Vibrational assignment

The observed transitions were assigned on the basis of the predictions of the effective ro-vibrational Hamiltonian developed by Teffo et al. [15,16]. The preliminary set of effective Hamiltonian parameters for $^{14}N^{15}N^{16}O$ was obtained by Vlasova et al. [17]. The adopted effective Hamiltonian is based on a polyad structure resulting from the approximate relations between the harmonic frequencies $\omega_3 \approx 2\omega_1 \approx 4\omega_2$. Due to the mixing between the normal mode $(V_1V_2^{\ell_2}V_3)$ vibrational states, it is preferable to label the energy levels using the triplet $\{P = 2V_1 + V_2 + 4V_3, \ell_2, i\}$ where the index i increases with the energy. We survey the vibrational assignments and the fraction relative to the $(V_1V_2^{\ell_2}V_3)$ dominant states of the present studied levels in Table 2.

All together 107 vibrational bands were assigned for $^{14}N^{15}N^{16}O$ in the studied region. Apart from the eight Π–Σ cold bands and four Σ–Π, two Δ–Π, one Π–Σ, one Φ–Δ hot bands, all the other analyzed bands are parallel bands ($\Delta l_2 = 0$): 36 Σ–Σ cold bands, 22 Σ–Σ hot bands, 23 Π–Π bands, and 10 Δ–Δ bands. For illustration, Fig. 2 presents the Q branch head of the perpendicular cold band (7 1 6)–(0 0 1) ($\{P, \ell_2, i\}$ notation) centered at 4406.129 cm^{-1}. Another example, R-branch of the parallel hot band (1 1 1 3)–(1 1 1) is shown in Fig. 3 together with the P-branch of the (1 0 0 3)–(0 0 1) band.

Table 1
Experimental conditions in the Fourier-transform measurements of the $^{14}N^{15}N^{16}O$ enriched sample

Detector	Pressure (Pa)	Path length (M)	Temperature (K)	Range (cm^{-1})	Resolution (cm^{-1})
Ge	1588	105	283	5000–9000	0.015
InSb	1654	87	283	3500–7500	0.015
InSb	1558	15	286	3300–4300	0.01
InSb	1558	105	284	3300–4300	0.01
InSb	1558	33	284	4100–5000	0.01
InSb	1558	105	283	4100–5000	0.01
InSb	1558	15	292	5000–6300	0.01
InSb	295	15	286	3300–4300	0.007
InSb	295	15	290	4100–5000	0.009
InSb	295	15	288	5000–6300	0.008
InSb	100	15	290	4100–5000	0.009

Table 2
Vibrational assignment and fractions respective to the basis states for the observed bands of $^{14}N^{15}N^{16}O$, in the 3500–9000 cm^{-1} FTS spectra

ΔP	Band[a]	(P, ℓ_2, i)[b]	ΔG_v (cm^{-1})	Basis states[c]	%Fraction[d]
Cold bands					
6	2200e–0000e	(604)	3568.5179	$22^0 0/06^0 0/14^0 0$	37/36/24
6	2200e–0000e (1400e–0000e)	(605)	3709.8141	$22^0 0/14^0 0/30^0 0$	35/34/24
6	3000e–0000e	(606)	3816.4740	$30^0 0/22^0 0$	72/22
7	0311e–0000e	(711)	3852.1636	$03^1 1$	86
7	1111e–0000e	(713)	3998.5721	$11^1 1$	86
7	1510e–0000e	(715)	4283.9571	$15^1 0/31^1 0/23^1 0$	37/35/17
7	3110e–0000e	(716)	4406.1291	$31^1 0/23^1 0$	57/32
8	0002e–0000e	(801)	4326.6170	$00^0 2$	99
8	0401e–0000e	(802)	4403.7291	$04^0 1/12^0 1$	76/22
8	1201e–0000e	(804)	4556.7668	$12^0 1/04^0 1$	62/22
8	2001e–0000e	(805)	4677.7977	$20^0 1$	82
8	0800e–0000e	(806)	4695.2757	$08^0 0/24^0 0$	42/40
8	3200e–0000e	(807)	4849.7622	$32^0 0/16^0 0/08^0 0$	41/34/16
8	2400e–0000e	(808)	4979.7020	$24^0 0/40^0 0/16^0 0$	33/32/16
8	4000e–0000e	(809)	5073.0681	$40^0 0/32^0 0$	60/28
9	0112e–0000e	(911)	4875.0669	$01^1 2$	99
9	2111e–0000e	(915)	5248.9484	$21^1 1/13^1 1$	71/24
10	0202e–0000e	(1001)	5417.8906	$02^0 2$	92
10	1002e–0000e	(1003)	5555.6452	$10^0 2$	91
10	0601e–0000e(2201e–0000e)	(1005)	5668.5504	$06^0 1/22^0 1/14^0 1$	35/35/25
10	2201e–0000e	(1006)	5808.9298	$22^0 1/14^0 1/30^0 1$	35/33/22
10	3001e–0000e	(1008)	5914.7100	$30^0 1/2^2 01$	71/22
10	3400e–0000e	(1009)	5977.2442	$34^0 0/0(10)^0 0/42^0 0/18^0 0$	26/25/22/19
10	4200e–0000e	(10010)	6121.7214	$42^0 0/18^0 0/26^0 0$	37/25/17
10	5000e–0000e(3400e–0000e)	(10011)	6240.6630	$50^0 0/34^0 0/26^0 0$	41/24/22
10	5000e–0000e	(10012)	6322.9963	$50^0 0/42^0 0/34^0 0$	45/32/16
11	1112e–0000e	(1113)	6108.6326	$11^1 2$	85
12	0003e–0000e	(1201)	6446.8932	$00^0 3$	98
12	1202e–0000e	(1204)	6653.9440	$12^0 2/04^0 2$	62/21
12	2002e–0000e	(1207)	6775.2209	$20^0 2$	80
12	1601e–0000e(0(12)00e–0000e)	(1208)	6923.4550	$16^0 1/0(12)^0 0$	22/19
12	1601e–0000e	(12010)	7051.7752	$24^0 1/40^0 1$	33/30
12	4001e–0000e	(12012)	7143.3954	$40^0 1/32^0 1$	57/28
12	6000e–0000e	(12015)	7492.1218	$60^0 0/36^0 0$	47/20
12	5200e–0000e	(12016)	7567.4296	$52^0 0/60^0 0/44^0 0$	30/29/22
13	0113e–0000e	(1311)	6981.8507	$01^1 3$	98
14	0203e–0000e	(1401)	7511.6378	$02^0 3$	91
14	1003e–0000e	(1403)	7650.7541	$10^0 3$	90
14	2202e–0000e	(1408)	7880.3901	$22^0 2/14^0 2/30^0 2$	36/32/20
14	3002e–0000e	(1409)	7985.5500	$30^0 2/22^0 2$	68/21
14	5001e–0000e(3401e–0000e)	(14014)	8284.8061	$50^0 1/34^0 1/26^0 1$	38/23/21
14	5001e–0000e	(14015)	8364.7025	$50^0 1/42^0 1/34^0 1$	40/24/16
16	0004e–0000e	(1601)	8538.5123	$00^0 4$	98
16	2003e–0000e	(1607)	8844.7205	$20^0 3$	78
Hot bands					
6	2001e–0200e	(805)	3533.4634	$20^0 1$	82
6	2310e–0110e	(714)	3559.3937	$23^1 0/07^1 0$	41/40
6	3200e–1000e	(807)	3569.4061	$32^0 0/16^0 0/08^0 0$	41/34/16
6	2400e–1000e	(808)	3699.3467	$24^0 0/40^0 0/16^0 0$	33/32/16
6	3200e–0200e	(807)	3705.4277	$32^0 0/16^0 0/08^0 0$	41/34/16
6	3220e–0220e(1620e–0220e)	(8212)	3707.5504	$32^2 0/16^2 0$	40/36
6	1510e–0110e	(715)	3708.5241	$15^1 0/31^1 0/23^1 0$	37/35/17
6	4000e–1000e	(809)	3792.7127	$40^0 0/32^0 0$	60/28
6	4110e–1110e	(919)	3807.8870	$41^1 0/33^1 0/25^1 0$	43/36/16
6	2400e–0200e	(808)	3835.3673	$24^0 0/40^0 0/16^0 0$	33/32/16
6	3220e–0220e	(8214)	3842.3883	$32^2 0/24^2 0$	47/38
6	4000e–0200e	(809)	3928.7337	$40^0 0/32^0 0$	60/28
7	0002e–0110e	(801)	3751.1835	$00^0 2$	99
7	3110e–0110e	(716)	3830.6956	$31^1 0/23^1 0$	57/32
7	2111e–1000e	(915)	3968.5934	$21^1 1/13^1 1$	71/24
7	1201e–0110e	(804)	3981.3326	$12^0 1/04^0 1$	62/22

(*continued on next page*)

Table 2 (*continued*)

ΔP	Band[a]	(P, ℓ_2, i)[b]	ΔG_v (cm^{-1})	Basis states[c]	%Fraction[d]
7	1221e–0110e	(8 2 3)	3989.2214	$12^21/04^21$	81/18
7	2001e–0110e	(8 0 5)	4102.3641	20^01	82
8	0222e–0220e	(10 2 2)	4272.8446	02^22	99
8	0202e–0200e	(10 0 1)	4273.5568	02^02	92
8	1002e–1000e	(10 0 3)	4275.2912	10^02	91
8	0112e–0110e	(9 1 1)	4299.6322	01^12	99
8	0511e–0110e	(9 1 2)	4380.8867	$05^11/13^11$	68/29
8	0601e–0200e(2201e–0200e)	(10 0 5)	4524.2168	$06^01/22^01/14^01$	35/35/25
8	1421e–0220e	(10 2 9)	4524.5216	$14^21/06^21/22^21$	34/33/30
8	2201e–1000e	(10 0 6)	4528.5754	$22^01/14^01/2^201$	35/33/22
8	1311e–0110e	(9 1 4)	4540.4254	$13^11/05^11/21^11$	45/29/24
8	3001e–1000e	(10 0 8)	4634.3560	$30^01/2^201$	71/22
8	2201e–0200e	(10 0 6)	4664.5962	$22^01/14^01/30^01$	35/33/22
8	2221e–0220e	(10 2 12)	4667.9681	$22^21/14^21$	56/31
8	2111e–0110e	(9 1 5)	4673.5140	$21^11/13^11$	71/24
8	3310e–0110e	(9 1 7)	4841.5391	$33^10/17^10/09^10$	37/28/21
8	5000e–1000e(3400e–1000e)	(10 0 11)	4960.3105	$50^00/34^00/26^00$	41/24/22
8	4200e–0200e	(10 0 10)	4977.3910	$42^00/18^00/26^00$	37/25/17
8	4110e–0110e(2510e–0110e)	(9 1 8)	4980.4324	$41^10/25^10/17^10$	41/29/21
8	4220e–0220e	(10 2 18)	4981.4847	$42^20/18^20/26^20$	44/25/23
8	5000e–1000e	(10 0 12)	5042.6443	$50^00/42^00/34^00$	45/32/16
8	4110e–0110e	(9 1 9)	5092.6452	$41^10/33^10/25^10$	43/36/16
8	5000e–0200e(3400e–0200e)	(10 0 11)	5096.3304	$50^00/34^00/26^00$	41/24/22
8	3420e–0220e	(10 2 20)	5108.2050	$34^20/42^20/26^20$	38/33/21
9	0332e–0220e	(11 3 2)	4821.9973	03^32	99
9	0202e–0110e	(10 0 1)	4842.4575	02^02	92
9	0222e–0110e	(10 2 2)	4848.4426	02^22	99
10	0312e–0110e	(11 1 1)	5386.1717	03^12	86
10	2002e–1000e	(12 0 7)	5494.8665	20^02	80
10	1202e–0200e	(12 0 4)	5509.6124	$12^02/04^02$	62/21
10	1222e–0220e	(12 2 7)	5510.4272	$12^22/04^22$	80/17
10	1112e–0110e	(11 1 3)	5533.2004	11^12	85
10	1511e–0110e	(11 1 6)	5794.7732	$15^11/31^11$	35/27
10	4001e–1000e	(12 0 12)	5863.0423	$40^01/32^01$	57/28
10	3221e–0220e	(12 2 18)	5914.1459	$32^21/24^21$	47/37
10	3111e–0110e	(11 1 8)	5915.5774	$31^11/23^11$	57/32
10	4310e–0110e(1910e–0110e)	(11 1 10)	6114.1471	$43^10/19^10/51^10$	26/26/19
10	5110e–0110e	(11 1 11)	6243.4646	$51^10/27^10$	44/24
10	4310e–0110e	(11 1 12)	6347.9112	$43^10/51^10/35^10$	35/30/23
12	0223e–0220e	(14 2 2)	6366.2447	02^23	98
12	0203e–0200e	(14 0 1)	6367.3023	02^03	91
12	1003e–1000e	(14 0 3)	6370.3973	10^03	90
12	0113e–0110e	(13 1 1)	6406.4208	01^13	98
12	2112e–0110e	(13 1 7)	6757.6784	$21^12/13^12$	71/23
13	4111e–0110e(2511e–01101e)	(13 1 10)	7039.7257	$41^11/25^11/17^11$	38/29/20
13	4111e–0110e	(13 1 12)	7149.7327	$41^11/33^11$	42/35
15	1113e–0110e	(15 1 3)	7615.0000	11^13	84

Notes:

[a] According to the maximum value of the modulo of the expansion coefficients of the eigenfunction. In the cases when there are two candidates for the same labeling or modulo of two principal expansion coefficients practically coincide we give in parentheses the second variant of the labeling.

[b] Cluster labeling notation: ($P = 2V_1 + V_2 + 4V_3$,ℓ_2,i) for the upper state of the band; i is the order number within the cluster increasing with the energy.

[c] Only basis states with modulo of expansion coefficients larger than 0.4 are presented.

[d] Squares of the expansion coefficients of the vibrational state for the dominant basis states appearing in the preceding column.

3.2. Band-by-band rotational analysis

The standard expression of the vibration-rotation energy levels was used for the fit of the spectroscopic parameters:

$$F_v(J) = G_v + B_vJ(J+1) - D_vJ^2(J+1)^2 + H_vJ^3(J+1)^3, \quad (1)$$

where G_v is the vibrational term value, B_v is the rotational constant, D_v and H_v are centrifugal distortion constants. The spectroscopic parameters for an upper state were fitted directly to the observed line positions of the respective band, and in the case of hot band involving e an f rotational levels, the *ee*, *ef*, *fe*, and *ff* sub-bands were considered, respectively. The lower state rotational constants were constrained to their literature values [7]. The observed line positions together with residuals are given in the Sup-

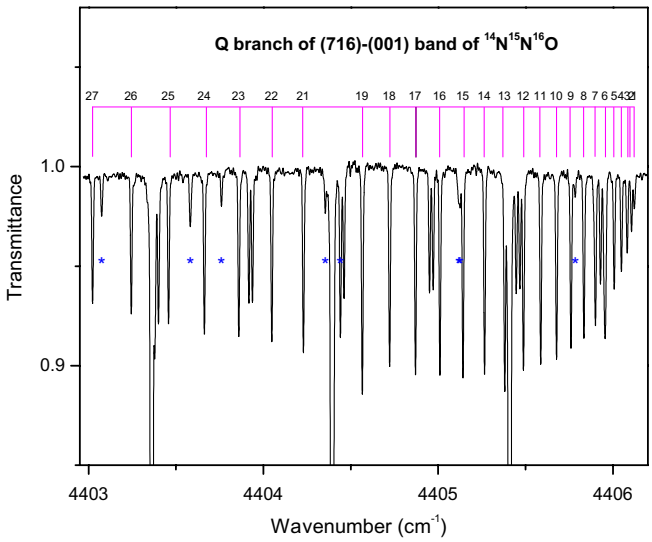

Fig. 2. The Q-branch of the perpendicular cold band (716)–(001) of $^{14}N^{15}N^{16}O$ centered at 4406.1291 cm^{-1}. The spectrum was recorded at a pressure of 1558 Pa and an equivalent absorption path length of 105 m. The rotational assignment is given. The lines marked by asterisks correspond to the (912)–(111) band transitions of $^{14}N^{15}N^{16}O$ centered at 4380.887cm^{-1}. Other lines belong to strong $^{14}N_2{}^{16}O$ bands.

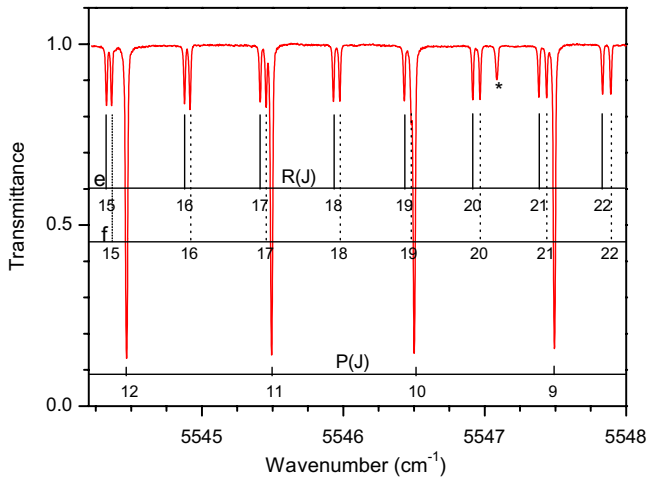

Fig. 3. The P-branch of the cold parallel band (1003)–(001) of $^{14}N^{15}N^{16}O$ centered at 5555.6452 cm^{-1} and the R- branch of the hot parallel band (1113)–(111) of $^{14}N^{15}N^{16}O$ centered at 5533.2004 cm^{-1}. The line marked by asterisk belongs to H_2O.

plementary material attached to this paper. The spectroscopic parameters retrieved from the fit of the line positions are listed in Table 3. The RMS values of the deviations (obs. − calc.) are in the order of 1.0×10^{-3} cm^{-1} which is consistent with the experimental accuracy of the line positions. For 27 bands reported in Refs. [5–13], our work extends to higher J value transitions and allows a refinement of the spectroscopic constants. They are reviewed and included in Table 3. Since some upper vibrational states have been reported through other bands, the corresponding bands and references are also indicated in the last column of Table 3 for completeness. Note that in some cases, several different bands can access the same upper vibrational state. For example, there are three bands (915)–(001), (915)–(111), (915)–(202) reaching the same (915) upper state at 5248.9477 cm^{-1}. In this case, the spectroscopic parameters of (915) state determined by (915)–(111) band with more observed lines and less RMS is preferable. Note that the vibrational states (1208) and (1116) are affected by very strong intrapolyad resonance interactions especially for those low J levels, so the spectroscopic constants of these two states were retrieved from the energy levels with high J values ($J'>18$ and $J'>20$, respectively).

4. Effective Hamiltonian

The effective Hamiltonian globally describing the vibration-rotation states of nitrous oxide molecule was discussed in Refs. [15,16,18–21]. Amat and Nielsen [18] and Amat et al. [19] have derived the effective Hamiltonian for triatomic linear molecules up to fourth-order perturbation theory without taking into account the accidental resonances. Pliva [20] developed the Hamiltonian including the resonance interaction terms for the N_2O molecule. Then Teffo and Chedin [21] added several higher-order resonance interaction terms to this effective Hamiltonian. Later Teffo et al. [15] considered the procedure of the reduction of this effective Hamiltonian.

The vibrational energy levels of N_2O molecule are grouped into the clusters. The clustering arises from the following approximate relations among the harmonic frequencies [20]:

$$\omega_3 \approx 2\omega_1 \approx 4\omega_2. \tag{2}$$

As a result, the vibrational states can be grouped into vibrational polyads with the pseudo-quantum number P:

$$P = 2V_1 + V_2 + 4V_3 \tag{3}$$

The effective Hamiltonian within the framework of the polyad model takes into account two types of accidental resonance interactions: anharmonic resonance interactions and anharmonic $+\ell$-type resonance interactions. The effective Hamiltonian can be presented by its matrix elements in the basis of the eigenfunctions of harmonic oscillators $|V_1V_2\ell_2V_3\rangle$ and rigid rotor $|JMK=\ell_2\rangle$ operators. Here V_i ($i=1$, 2, and 3) are the principal vibrational quantum numbers, ℓ_2 is the vibrational angular momentum quantum number, J and K are the quantum numbers of the total angular momentum and its projection on the molecular-fixed z axis. Below we give the diagonal matrix elements and the off-diagonal matrix elements of resonance interactions which have been taken into account in this paper.

Table 3
Spectroscopic parameters (in cm^{-1}) of the rovibrational bands of $^{14}N^{15}N^{16}O$ assigned in the *FTS* spectra between 3500 and 9000 cm^{-1}

ΔG_v[a]	Type	Bands[b]	(P,ℓ_2,i)[c]	G_v	B_v	$D_v \times 10^7$	$H_v \times 10^{12}$	Observed lines	n/N[d]	RMS $\times 10^3$	Previous works[e]
Cold bands											
3568.51790(15)	Σ–Σ	2200e–0000e	(604)	3568.51790(15)	0.41880608 (56)	4.8395 (46)	26.09 (10)	P58/R55	111/113	0.72	
3568.5196(2)		*1400e–0000e^A*		*3568.5196(2)*	*0.4188049(14)*	*4.755(29)*	*20.1(15)*	*P32/R35*	*59*	*0.5*	
3709.814094(49)	Σ–Σ	2200e–0000e (1400e–0000e)	(605)	3709.814094(49)	0.41625839(12)	2.87387(65)	4.4164(95)	P71/R70	136/138	0.26	
3709.81275(27)		*2200e–0000e^T*		*3709.81275(27)*	*0.416264779(252)*	*2.76743(287)*	*7.042(114)*				
3816.474006(97)	Σ–Σ	3000e–0000e	(606)	3816.474006(97)	0.41352652(22)	1.7017(11)	0.702(15)	P72/R73	135/144	0.52	
3816.47539(15)		*3000e–0000e^T*		*3816.47539(15)*	*0.413525995(482)*	*1.68017(827)*	*1.250(253)*				
3852.16361 (27)	Π–Σ	0311e–0000e	(711)	3852.16361 (27)	0.4163685(14)	2.276(19)	4.75(67)	P44/R43	49/57	0.75	*0311e–0110e^T*
3852.16339 (60)		0311f–0000e		3852.16440(45)	0.4179044(16)	2.3667(77)	2.28(30)	Q45	21/23	1.00	*0311f–0110f^T*
3998.572117(61)	Π–Σ	1111e–0000e	(713)	3998.572117(61)	0.41399004(17)	1.7639(11)	0.075(18)	P65/R64	123/128	0.30	*1111e–0110e^A*
3998.5732(2)		*1111e–0000e^A*		*3998.5732(2)*	*0.4139892(13)*	*1.738(15)*		*P31/R24*	*40*	*0.53*	
3998.57268(12)		1111f–0000e		3998.57268(12)	0.4148567(19)	1.73836(53)	−0.167(68)	Q62	58/60	0.49	*1111f–0110f^A*
4283.95710(56)	Π–Σ	1510e–0000e	(715)	4283.95710(56)	0.4157690(16)	2.1311(97)		P34/R39	22/43	0.94	*1510e–0110e^A*
4283.95910(54)		1510f–0000e		4283.95910(54)	0.4175723(22)	2.183(16)		Q36	20/21	1.02	*1510f–0110f^A*
4326.617006(46)	Σ–Σ	0002e–0000e	(801)	4326.617006(46)	0.412317205(95)	1.74814(44)	−0.0125(54)	P81/R75	139/155	0.25	
4326.61717(5)		*0002e–0000e^T*		*4326.61717(5)*	*0.412317083(77)*	*1.748183(150)*					
4403.72906(26)	Σ–Σ	0401e–0000e (perturbed[g])	(802)	4403.7290621788	0.4175093(11)	5.013(10)	31.48(24)	P53/R53	93/104	1.10	*0401e–0200e^A*
4406.12908(21)	Π–Σ	3110e–0000e (perturbed[g])	(716)	4406.12908(21)	0.4137143(11)	1.761 (11)	2.27(30)	P26/R52	63/75	0.80	*3110e–0110e^T*
4406.12896(16)		3110f–0000e		4406.12896(16)	0.41485580(45)	1.5659(23)		Q46	41/41	0.55	*3110f–0110e^T*
4556.766752(98)	Σ–Σ	1201e–0000e	(804)	4556.766752(98)	0.41483979(27)	2.7361(16)	5.137(27)	P67/R65	124/132	0.50	
4677.797746(37)	Σ–Σ	2001e–0000e	(805)	4677.797746(37	0.411952697(81)	1.72026(41)	0.2688(53)	P76/R60	130/137	0.20	
4677.79785(5)		*2001e–0000e^T*		*4677.79785(5)*	*0.411950301(410)*	*1.68900(446)*	*-0.771(113)*				
4695.27567(26)	Σ–Σ	0800e–0000e	(806)	4695.27567(26)	0.4193856(15)	8.222(18)	82.03(60)	P33/R45	54/61	0.84	
4849.762229(83)	Σ–Σ	3200e–0000e	(807)	4849.762229(83)	0.41691237(31)	4.7031(26)	23.069(59)	P58/R56	107/113	0.38	
4875.066916(64)	Π–Σ	0112e–0000e	(911)	4875.066916(64)	0.41253118(22)	1.7652(17)	−0.059(35)	P60/R58	112/119	0.30	*0112e–0110e^A*
4875.06578(39)		*0112e–0000e^T*		*4875.06578(39)*	*0.412533725(51)*	*1.787208(920)*					
4875.067006(90)		0112f–0000e		4875.067006(90)	0.41331100(16)	1.77717(51)	−0.111(56)	Q59	57/57	0.36	*0112f–0110f^A*
4875.06565(34)		*0112f–0000e^T*		*4875.06565(34)*	*0.413312999(394)*	*1.79663(251)*					
4979.701973(45)	Σ–Σ	2400e–0000e	(808)	4979.701973(45)	0.41440082(14)	2.6182(10)	3.951(19)	P62/R60	121/125	0.22	
4979.70261(75)		*3200e–0000e^T*		*4979.70261(75)*	*0.414391046(3167)*	*2.4745(530)*					
5073.068063(71)	Σ–Σ	4000e–0000e	(809)	5073.068063(71)	0.41186316(22)	1.5308(15)	1.606(29)	P64/R60	117/123	0.35	
5073.06705(70)		*4000e–0000e^T*		*5073.06705(70)*	*0.411861029(294)*	*1.49116(471)*					
5248.94842(44)	Π–Σ	2111e–0000e	(915)	5248.94842(44)	0.4121863(18)	1.735(14)		P38/R24	34/39	1.05	*2111e–0110e^A*
5248.94821(31)		2111f–0000e		5248.94821(31)	0.4131563(18)	1.712(21)		Q30	23/27	0.72	*2111f–0110e^A*
5417.89062(13)	Σ–Σ	0202e–0000e	(1001)	5417.89062(13)	0.41340691(78)	2.832(10)	6.13(37)	P45/R43	81/83	0.52	
5555.645161(69)	Σ–Σ	1002e–0000e	(1003)	5555.645161(69)	0.41045015(21)	1.7420(14)	0.135(26)	P63/R62	119/125	0.34	
5555.6463(1)		*1002e–0000e^A*		*5555.6463(1)*	*0.4104490(7)*	*1.724(6)*		*P30/R33*	*53*	*0.49*	
5668.55036(14)	Σ–Σ	0601e–0000e (2201e–0000e)	(1005)	5668.55036(14)	0.41565110(93)	4.856(14)	27.89(57)	P39/R41	79/81	0.55	
5808.929817(42)	Σ–Σ	2201e–0000e	(1006)	5808.929817(42)	0.41301693(17)	2.7048(16)	5.31(39)	P56/R57	106/114	0.19	
5914.710035(43)	Σ–Σ	3001e–0000e	(1008)	5914.710035(43)	0.41016992(15)	1.6501(29)	0.705(25)	P60/R60	110/120	0.21	
5914.70926(196)		*3001e–0000e-^{T}*		*5914.70926(196)*	*0.410158758(1469)*	*1.4536(710)*					
5977.24422(45)	Σ–Σ	3400e–0000e	(1009)	5977.24422(45)	0.4174135(41)	8.139(91)	83.2(55)	P31/R33	50/57	1.17	
6108.63257(33)	Π–Σ	1112e–0000e	(1113)	6108.63257(33)	0.4107056(25)	1.882(44)	5.8(21)	P39/R31	58/63	0.98	

6108.63353(31)		1112f–0000e		6108.63353(31)	0.4115464(13)	1.7531(96)		Q37	33/35	0.87
6121.72139(11)	Σ–Σ	4200e–0000e	(10010)	6121.72139(11)	0.41498187(54)	4.5291(61)	19.77(18)	P48/R48	91/96	0.47
6121.72228(46)		*4200e–0000e*^{L}		*6121.72228(46)*	*0.414984(31)*	*4.566(51)*	*22.0(23)*	*P38/R38*	*56/61*	*1.3*
6240.662956(73)	Σ–Σ	5000e–0000e (3400e–0000e)	(10011)	6240.662956(73)	0.41247604(28)	2.5585(24)	3.85(53)	P55/R55	108/111	0.34
6240.66496(25)		*5000e–0000e*^{L}		*6240.66496(25)*	*0.41246940(79)*	*2.4543(44)*		*P42/R45*	*70/76*	*1.2*
6322.996268(44)	Σ–Σ	5000e–0000e	(10012)	6322.996268(44)	0.41039770(20)	1.2539(21)	3.18(57)	P52/R50	98/103	0.19
6322.99842(46)		*5000e–0000e*^{L}		*6322.99842(46)*	*0.41039030(70)*	*1.1568(34)*		*P44/R48*	*68/71*	*1.1*
6446.893234(96)	Σ–Σ	0003e–0000e	(1201)	6446.893234(96)	0.40897246(27)	1.7411(18)	−6.321(30)	P66/R60	117/127	0.48
6446.89423		*0003e–0000e*^{W}		*6446.89423*	*0.4089692*	*1.730*				
6446.89417(18)		*0003e–0000e*^{L}		*6446.89417(18)*	*0.40897230(31)*	*1.74229(94)*		*P58/R60*	*106/109*	*1.0*
6653.94404(18)	Σ–Σ	1202e–0000e	(1204)	6653.94404(18)	0.4115826(11)	2.736(17)	5.34(68)	P41/R41	81/81	0.66
6653.94605(60)		*1202e–0000e*^{L}		*6653.94605(60)*	*0.4115745(23)*	*2.605(17)*		*P39/R38*	*48/50*	*1.9*
6775.22091(28)	Σ–Σ	2002e–0000e (perturbed[f])	(1207)	6775.22091(28)	0.4086088(19)	1.848(20)	4.70(55)	P51/R51	69/102	1.11
6775.22182(33)		*2002e–0000e*^{L}		*6775.22182(33)*	*0.4085965(38)*	*1.266(81)*		*P46/R47*	*35/79*	*1.0*
6923.4550(33)	Σ–Σ	1601e–0000e (0(12)00e–0000e) (perturbed[f])	(1208)	6923.4550(33)	0.4139777(11)	5.431(81)		P33/R31	20/54	0.81
6981.85068(81)	Π–Σ	0113e–0000e	(1311)	6981.85068(81)	0.4092471(44)	1.919(44)		P32/R20	31/38	1.61
6981.85330(45)		0113f–0000e		6981.85330(45)	0.4100078(27)	1.927(29)		Q32	26/30	1.1
7051.77452(94)	Σ–Σ	1601e–0000e	(12010)	7051.77452(94)	0.41114508(47)	2.5633(55)	3.71(17)	P49/R47	92/95	0.39
7143.39539(15)	Σ–Σ	4001e–0000e	(12012)	7143.39539(15)	0.40850952(63)	1.4844(62)	1.52(16)	P53/R50	100/103	0.64
7492.12183(24)	Σ–Σ	6000e–0000e	(12015)	7492.12183(24)	0.4104420(13)	2.443(15)	3.31(51)	P43/R46	85/89	0.95
7511.63778(32)	Σ–Σ	0203e–0000e	(1401)	7511.63778(32)	0.4101315(17)	2.669(21)	−2.95(67)	P39/R47	76/87	1.27
7567.42959(33)	Σ–Σ	5200e–0000e	(12016)	7567.42959(33)	0.4092254(24)	0.778(41)	5.6(19)	P40/R37	73/77	1.14
7650.754129(91)	Σ–Σ	1003e–0000e	(1403)	7650.754129(91)	0.40710222(34)	1.7366(28)	0.125(62)	P59/R55	110/115	0.43
7880.39008(29)	Σ–Σ	2202e–0000e	(1408)	7880.39008(29)	0.4097388(16)	2.392(16)		P33/R32	60/68	1.00
7985.54955(20)	Σ–Σ	3002e–0000e	(1409)	7985.54955(20)	0.4068065(12)	1.562(17)	−2.32(63)	P44/R43	81/87	0.79
8284.80614(60)	Σ–Σ	5001e–0000e (3401e–0000e)	(14014)	8284.80614(60)	0.4091799(39)	1.572(50)		P30/R27	45/54	1.73
8364.70253(51)	Σ–Σ	5001e–0000e	(14015)	8364.70253(51)	0.4071471(47)	2.26(10)	65.9(61)	P30/R33	54/60	1.38
8538.51227(24)	Σ–Σ	0004e–0000e	(1601)	8538.51227(24)	0.40562280(99)	1.7231(92)	−1.02(22)	P55/R49	97/104	1.08
8844.72048(24)	Σ–Σ	2003e–0000e	(1607)	8844.72048(24)	0.40524281(91)	1.6772(63)		P42/R34	67/76	1.01

Notes.

The lower state constants and those appear between square brackets were fixed at the values of Ref. [9]. The uncertainties are given in parenthesis in the unit of the last quoted digit. When a given band has been previously analyzed, the corresponding spectroscopic parameters are given in italics for comparison: ^{T}Toth [9], ^{A}Amiot [5], ^{H}Herbin [11] ^{L}Liu et al. [12,13], ^{W}Wang [10].

The cold and hot bands are listed successively and ordered according to their ΔG_v values.

[a] Difference between the upper and lower vibrational term values.

[b] Normal mode labeling according to the maximum value of the modulo of the expansion coefficients of an eigenfunction. In the cases when there are two candidates for the same labeling or modulo of two principal expansion coefficients practically coincide, we give in parentheses the second variant of the labeling. Note that as a result of strong vibrational mixing, the normal mode labeling of some states differs from that given in the previous analysis.

[c] Cluster labeling notation: ($P = 2V_1 + V_2 + 4V_3,\ell_2$, i) for the upper state of the band; i is the order number within the cluster increasing with the energy.

[d] n: number of transitions included in the fit; N: number of assigned rotational transitions.

[e] Previous observations of the upper level through a different transition.

[f] Bands perturbed by intrapolyad anharmonic interaction (see text).

[g] Bands perturbed by resonance interactions (see text). Only part of the rotational levels was used as input data of the fit.

(*continued on next page*)

Table 3 (*continued*)

ΔG_v[a]	Type	Bands[b]	(P,ℓ_2,i)[c]	G_v	B_v	$D_v \times 10^7$	$H_v \times 10^{12}$	Observed lines	n/N[d]	RMS $\times 10^3$	Previous works[e]
Hot bands											
3533.46335(24)	Σ–Σ	2001e–0200e	(805)	4677.79673(24)	0.4119587(23)	1.840(49)	6.1(28)	P34/R34	58/61	0.79	
3559.393658(97)	Π–Π	2310e–0110e	(714)	4134.827308(97)	0.41791801(37)	2.8498(33)	7.146(79)	P52/R54	89/101	0.39	
3559.393281(92)		2310f–0110f		4134.826931(92)	0.42035823(40)	3.0098(39)	−3.87(10)	P54/R51	89/102	0.36	
3569.40615(79)	Σ–Σ	3200e–1000e	(807)	4849.76027(79)	0.4169174 (31)	4.774(32)	25.07(94)	P49/R39	42/54	1.43	
3699.346706(87)	Σ–Σ	2400e–1000e	(808)	4979.700826(87)	0.41440060(44)	2.6166(52)	3.92(16)	P49/R47	79/90	0.34	
3705.42766(17)	Σ–Σ	3200e–0200e	(807)	4849.76104(17)	0.41691380(70)	4.7219(69)	23.74(18)	P53/R49	79/84	0.64	
3707.55038(26)	Δ–Δ	1620e–0220e	(8212)	4858.58128(26)	0.4171138(11)	−4.212(12)	−15.81(33)	P51/R43	66/74	0.85	
3707.55180(25)		1620f–0220f		4858.58270(25)	0.4171160(11)	2.171(12)	0.68(36)	P49/R47	71/82	0.82	
3708.524111(81)	Π–Π	1510e–0110e	(715)	4283.957761(81)	0.41577087(24)	2.1730(16)	1.747(30)	P68/R66	107/122	0.36	
3708.5256(1)		*2310e–0110e*[A]		*4283.9592(1)*	*0.4157711(5)*	*2.153(16)*		*P30/Rr31*	*44*	*0.28*	
3708.523789(70)		1510f–0110f		4283.957439(70)	0.41757649(26)	2.2087(13)	−0.104(22)	P66/R66	109/126	0.32	
3708.5256(1)		*2310f–0110f*[A]		*4283.9592(1)*	*0.4175759(9)*	*2.206(7)*		*P31/R29*	*47*	*0.36*	
3751.18349(40)	Σ–Π	0002e–0110e	(801)	4326.61714(40)	0.4123165(27)	1.7458(53)		P46/R46	50/59	1.52	*0002e–0000e*[A]*0002e–0000e*[T]
3751.18357(33)		0002e–0110f		4326.61722(33)	0.4123165(14)	1.748(11)		Q37	22/26	0.83	
3792.712731(66)	Σ–Σ	4000e–1000e	(809)	5073.066851(66)	0.41186226(29)	1.5214(29)	1.362(74)	P52/R51	89/95	0.28	*4000e–0000e*[T]
3807.88695(25)	Π–Π	4110e–1110e	(919)	5668.07816(25)	0.41202934(91)	1.5944(60)		P41/R37	47/57	0.82	
3807.88786(22)		4110f–1110f		5668.07907(22)	0.41337779(70)	1.3754(41)		P44/R38	43/54	0.71	
3830.69556(18)	Π–Π	3110e–0110e (perturbed[g])	(716)	4406.12921(18)	0.41370754(49)	1.6859(29)	0.222(46)	P66/R66	102/124	0.81	
3830.69679(81)		*3110e–0110e*[T]		*4406.13044(81)*	*0.41371590(1737)*	*2.003(418)*	*13.8(271)*				
3830.69520(43)		3110e–0110f (perturbed[g])		4406.12885(43)	0.4136998 (42)	1.357(74)		Q25	18/23	0.97	
3830.69507(35)		3110f–0110e		4406.12872(35)	0.4148564(25)	1.564(33)		Q27	16/21	0.63	
3830.69498(12)		3110f–0110f		4406.12863(12)	0.41485654(29)	1.5822(16)	0.726(24)	P71/R69	123/134	0.58	
3830.69498(85)		*3110f–0110f*[T]		*4406.12709(85)*	*0.414864194(3733)*	*1.7352(777)*	*9.71(473)*				
3835.367271(86)	Σ–Σ	2400e–0200e	(808)	4979.700651(86)	0.41440161(40)	2.6282(38)	4.345(98)	R52/P52	83/91	0.38	
3842.38830(24)	Δ–Δ	3220e–0220e	(8214)	4993.41920(24)	0.4149310(12)	1.092(18)	4.07(38)	P50/R45	67/78	0.87	
3842.38868(22)		3220f–0220f		4993.41958(22)	0.4149238(10)	1.601(11)	−0.55(30)	P50/R49	75/83	0.79	
3928.73374 (16)	Σ–Σ	4000e–0200e	(809)	5073.06712 (16)	0.41186112(89)	1.504(11)	0.61 (36)	P47/R45	70/83	0.54	*4000e–0000e*[A]
3968.59336(77)	Π–Σ	2111e–1000e	(915)	5248.94748(77)	0.4121891(30)	1.748(24)	[0.04195]	P36/R25	36/40	1.53	*2111e–0110e*[A]
3968.59497(42)		2111f–1000e		5248.94909(42)	0.413152(20)	1.658(16)	[0.04195]	Q35	31/32	1.18	*2111f–0110f*[A]
3981.33262(16)	Σ–Π	1201e–0110e	(804)	4556.76627(16)	0.41484235(62)	2.7638(57)	5.81(14)	P55/R52	90/98	0.63	
3981.33378(16)		*1201e–0110e*[H]		*4556.76743(16)*	*0.41483484(32)*	*2.63166(86)*		*P63/R34*	*49*	*0.6*	
3981.33377(23)		1201e–0110f		4556.76642(23)	0.41483120(70)	2.6021(40)		Q48	40/45	0.70	
3981.33417(18)		*1201e–0110f*[H]		*4556.76*682(18)				Q46	39	0.6	
3989.22032(33)	Δ–Π	1221e–0110f	(823)	4564.65397(33)	0.41503770(96)	1.0072(53)		Q46	40/45	0.99	
3989.22134(26)		1221f–0110e		4564.65499(26)	0.41502810(62)	1.7601(27)		Q49	45/48	0.87	
3989.22137(15)		1221e–0110e		4564.65502(15)	0.41502955(76)	0.8928(88)	−4.05(28)	P48/R44	79/86	0.51	
3989.221864(97)		1221f–0110f		4564.655514(97)	0.4150279(22)	1.76806(94)		P53/R47	83/92	0.44	
4102.36410(13)	Σ–Π	2001e–0110e	(805)	4677.79775(13)	0.41195210(47)	1.7138(32)		P42/R32	68/70	0.56	*2001e–0000e*[T]
4102.36408(12)		2001e–0110f		4677.79773(12)	0.41195180(32)	1.7032(17)		Q46	44/46	0.41	
4272.84460(22)	Δ–Δ	0222e–0220e	(1022)	5423.87550(22)	0.4135216(12)	1.120(14)	3.81(43)	P28/R47	59/67	0.81	
4273.55684(14)	Σ–Σ	0202e–0200e	(1001)	5417.89022(14)	0.41340978(52)	2.8743(45)	7.66(10)	P57/R48	103/105	0.63	
4275.291150(74)	Σ–Σ	1002e -1000e	(1003)	5555.645270(74)	0.41044960(16)	1.73635(59)	[0.047195]	P55/R52	89/95	0.37	*1002e–0000e*[A]
4299.632225(69)	Π–Π	0112e–0110e	(911)	4875.065875(69)	0.412531872(88)	1.76935(19)		P72/R68	106/131	0.36	*0112e–0000e*[T]
4299.6344(1)		*0112e–0110e*[A]		*4875.0681(1)*	*0.4125320(2)*	*1.768(1)*		*P44/R38*	*59*	*0.2*	
4299.63259(32)		0112e–0110f		4875.06624(32)	0.4125343(27)	1.807(41)		Q25	17/22	0.58	
4299.632222(83)		0112f–0110f		4875.065872(83)	0.41331165(19)	1.7804(10)	−0.024(14)	P72/R64	101/129	0.34	*0112f–0000e*[T]

4299.6344(1)		*0112f–0110f*[A]		*4875.0681(1)*	*0.4133117(2)*	*1.782(1)*		*P43/R40*	*63*	*0.24*
4299.63266(26)		0112f–0110e		4875.06631(26)	0.4133109(15)	1.763(16)		Q32	20/28	0.56
4380.88670(21)	Π–Π	0511e–0110e	(912)	4956.32035(21)	0.4167787(14)	2.882(21)	8.73(83)	P42/R41	66/73	0.71
4380.88624(17)		0511f–0110f		4956.31989(17)	0.4190311(10)	3.111(11)		P33/R31	57/59	0.65
4524.216809(94)	Σ–Σ	0601e–0200e (2201e–0220e)	(1005)	5668.550189(94)	0.41565245(53)	0.4878(70)	28.91(24)	P47/R43	76/79	0.36
4524.52157(21)	Δ–Δ	1421e–0220e	(1029)	5675.55247(21)	0.4157805(10)	−0.546(11)	−20.16(33)	P50/R48	79/91	0.81
4524.52264(18)		1421f–0220f		5675.55354(18)	0.41578318(82)	2.1841(89)	0.35(25)	P51/R49	80/92	0.67
4528.57535(20)	Σ–Σ	2201e–1000e	(1006)	5808.92947(20)	0.4130190(13)	2.748(19)	7.39(77)	P42/R40	64/70	0.64
4540.425422(52)	Π–Π	1311e–0110e	(914)	5115.859072(52)	0.41448785(19)	2.1851(16)	2.242(37)	P56/R53	99/104	0.20
4540.425416(54)		1311f–0110f		5115.859066(54)	0.41611889(20)	2.2357(18)	−0.306(44)	P55/R53	98/104	0.22
4634.355912(76)	Σ–Σ	3001e–1000e	(1008)	5914.710032(76)	0.41016931(30)	1.6453(28)	0.607(67)	P55/R53	96/99	0.33
4664.596188(76)	Σ–Σ	2201e–0200e	(1006)	5808.929568(76)	0.41301908(39)	2.7384(46)	6.57(14)	P49/R45	77/83	0.29
4667.96814(78)	Δ–Δ	2221e–0220e	(10212)	5818.99904(18)	0.4135034(77)	3.97(19)	16.2(13)	P32/R31	44/49	1.39
4667.97073(90)		2221f–0220f		5819.00163(90)	0.4134736(86)	3.96(21)	11.4(14)	P33/R31	41/51	1.46
4673.51403(14)	Π–Π	2111e–0110e	(915)	5248.94768(14)	0.41218815(44)	1.7488(32)	0.412(63)	P61/R57	106/113	0.59
4673.5170(1)		*2111e–0110e*[A]		*5248.9507(1)*	*0.4125320(2)*	*1.768(1)*	*1.2(4)*	*P42/R36*	*58*	*0.31*
4673.51566(15)		2111f–0110f		5248.94932(15)	0.41315355(44)	1.6812(31)	0.320(60)	P62/R58	107/112	0.61
4673.5170(1)		*2111f–0110f*[A]		*5248.9507(1)*	*0.4131542(3)*	*1.679(2)*	*1.2(4)*	*P42/R35*	*57*	*0.27*
4821.99722(50)	Φ–Δ	0332e–0220f	(1132)	5973.02812(50)	0.4141109(17)	1.532(11)		Q40	27/34	1.25
4821.99728(83)		0332e–0220e		5973.02818(83)	0.4141256(93)	1.82(20)		P16/R20	25/25	1.52
4822.00002(52)		0332f–0220e		5973.03092(52)	0.4140954(16)	1.3921(97)		Q42	31/35	1.37
4841.53903(17)	Π–Π	3310e–0110e	(917)	5416.97268(17)	0.41592060 (88)	2.822(10)	6.41(31)	P48/R46	76/83	0.63
4841.53899(13)		3310f–0110f		5416.97264(13)	0.41851225(60)	2.9320(67)	−3.93(20)	P50/R47	77/85	0.47
4842.45753(17)	Σ–Π	0202e–0110e	(1001)	5417.89118(17)	0.41340835(86)	2.851(10)	6.72(33)	P48/R46	77/85	0.62
4842.45864(28)		0202e–0110f		5417.89229(28)	0.4133970(90)	2.6740(54)		Q43	37/38	0.91
4848.44261(19)	Δ–Π	0222e–0110e	(1022)	5423.87626(19)	0.4135157(11)	0.765(16)	−7.52(58)	P44/R41	70/75	0.64
4848.44254(19)		0222f–0110f		5423.87619(19)	0.41351810(60)	1.8009(33)		P45/R42	71/74	0.81
4848.44195(30)		0222e–0110f		5423.87460(30)	0.4135237(11)	0.9249(75)		Q42	34/40	0.83
4848.44203(17)		0222f–0110e		5423.87468(17)	0.41351920(45)	1.8061(28)		Q45	38/39	0.49
4960.31053(21)	Σ–Σ	5000e–1000e (3400e–1000e)	(10011)	6240.6646(21)	0.4124761(12)	2.559(16)	4.15(57)	P44/R43	71/81	0.65
4977.39104(32)	Σ–Σ	4200e–0200e	(10010)	6121.72442(32)	0.4149727(25)	4.36(46)	11.7(22)	P38/R37	59/68	1.0
4980.432359(64)	Π–Π	4110e–0110e (2510e–0110e)	(918)	5555.866009(64)	0.41385377(27)	2.1555(27)	1.780(73)	P53/R48	91/97	0.26
4980.432074(99)		4110f–0110f (2510f–0110f)		5555.865724(99)	0.41580456(39)	2.1667(35)	3.490(82)	P54/R53	92/97	0.39
4981.48472(71)	Δ–Δ	4220e–0220e	(10218)	6132.51562(71)	0.415334(10)	2.68(35)	139(32)	P29/R23	36/41	1.48
4981.48583(39)		4220f–0220f		6132.51673(39)	0.4152907(31)	0.753(56)	−6.6(27)	P39/R20	44/51	1.08
5042.64431(19)	Σ–Σ	5000e–1000e	(10012)	6322.99843(19)	0.4103961(12)	1.226(18)	1.95(69)	P43/R41	74/79	0.69
5092.64521(10)	Π–Π	4110e–0110e	(919)	5668.07886(10)	0.41202722(23)	1.57945(96)		P52/R51	89/96	0.46
5092.64528(11)		4110f–0110f		5668.07893(11)	0.41337905(43)	1.4102(41)	1.50(10)	P53/R53	97/103	0.42
5096.33045(39)	Σ–Σ	5000e–0200e (3400e–0200e)	(10011)	6240.66383(39)	0.4124794(28)	2.661(50)	10.4(25)	P34/R37	43/48	0.80
5108.20497(34)	Δ–Δ	3420e–0220e	(10220)	6259.23587(34)	0.4133865(29)	1.375(58)	17.7(31)	P36/R36	56/63	0.93
5386.17173(59)	Π–Π	0312e–0110e	(1111)	5961.60538(59)	0.413197(10)	3.75(43)	175(51)	P24/R22	33/41	0.98
5386.17284(34)		0312f–0110f		5961.60649(34)	0.4146681(17)	2.326(18)		P36/R31	52/57	1.11
5494.86653(52)	Σ–Σ	2002e–1000e (perturbed[f])	(1207)	6775.22065(52)	0.4086241(39)	2.211(60)	22.7(25)	P41/R38	54/74	1.63
5509.61244(32)	Σ–Σ	1202e–0200e	(1204)	6653.94582(32)	0.4115775(22)	2.628(27)	[6.67960]	P31/R28	47/53	1.05
5510.42715(48)	Δ–Δ	1222e–0220e	(1227)	6661.45805(48)	0.4117605(37)	0.781(57)		P30/R27	37/46	1.22

(*continued on next page*)

Table 3 (*continued*)

ΔG_v[a]	Type	Bands[b]	(P,ℓ_2,i)[c]	G_v	B_v	$D_v \times 10^7$	$H_v \times 10^{12}$	Observed lines	n/N[d]	RMS $\times 10^3$	Previous works[e]
5533.20040(27)	Π–Π	1112e–0110e	(1113)	6108.63405(27)	0.4107034(15)	1.829(20)	3.10(71)	P47/R44	75/88	0.87	
5533.20235(28)		1112f–0110f		6108.63600(28)	0.4115408 (15)	1.675(20)	−2.68(71)	P49/R47	81/93	0.97	
5794.7732(10)	Π–Π	1511e–0110e (perturbed[f])	(1116)	6370.2069 (10)	0.4126366(20)	2.2327(90)		P44/R43	40/82	0.87	
5794.78341(96)		1511f–0110f (perturbed[f])		6370.21706(96)	0.4143751(19)	2.2855(81)		P44/R42	39/81	0.80	
5863.04226(34)	Σ–Σ	4001e–1000e	(12012)	7143.39638(34)	0.4085098(30)	1.539(63)	6.6(35)	P36/R34	53/63	0.89	
5914.14591(36)	Δ–Δ	3221e–0220e	(12218)	7065.17681 (36)	0.4116929(30)	0.827 (29)		P24/R29	39/45	1.05	
5915.57732(12)	Π–Π	3111e–0110e	(1118)	6491.01097(12)	0.41043540(28)	1.6622(12)		P52/R52	81/97	0.53	
5915.57505(53)		*3111e–0110e*[L]		*6491.00870(53)*	*0.4104273(28)*	*1.551(28)*		*P10/R31*	*15/20*	*0.9*	
5915.57673(17)		3110f–0110f		6491.01038(17)	0.41154629(74)	1.5827(77)	1.42(22)	P53/R49	82/94	0.56	
5915.57408(52)		*3110f–0110f*[L]		*6491.00773(52)*	*0.4115402(38)*	*1.419(67)*	*-6.8(30)*	*P10/R38*	*25/27*	*1.0*	
6114.14709(44)	Π–Π	4310e–0110e (1910e–0110e)	(11110)	6689.58074(44)	0.4138794(20)	2.681(18)		P31/R33	44/52	1.18	
6114.14712(44)		4310f–0110f (1910f–0110f)		6689.58077(44)	0.4166468(22)	2.933(21)		P30/R33	42/50	1.09	
6243.46456(22)	Π–Π	5110e–0110e	(11111)	6818.89821(22)	0.41191414(76)	2.0837(48)		P43/R41	71/78	0.92	
6243.46665(42)		*5110e–0110e*[L]		*6818.90026(42)*	*0.411909(17)*	*2.053(13)*		*P32/R36*	*32/35*	*1.0*	
6243.46404(22)		5110f–0110f		6818.89769(22)	0.41403098(73)	2.0913(49)		P44/R42	69/78	0.89	
6243.46586(61)		*5110f–0110f*[L]		*6818.89951(61)*	*0.4140284(36)*	*2.049(41)*		*P32/R23*	*30/34*	*1.4*	
6347.91120(35)	Π–Π	4310e–0110e	(11112)	6923.34485(35)	0.4104470(18)	1.362(25)	−3.00(93)	P43/R41	64/74	0.87	
6347.91376(26)		4310f–0110f		6923.34741(26)	0.4120765(18)	1.135(29)	1.5(12)	P41/R40	67/80	0.85	
6366.24468(45)	Δ–Δ	0223e–0220e	(1422)	7517.27558(45)	0.4102530(40)	1.007(89)	−7.9(51)	P28/R34	48/58	1.22	
6366.24524(56)		*0223e–0220e*[L]		*7517.27614(56)*	*0.4102588(25)*	*1.129(22)*		*P26/R34*	*38/38*	*1.4*	
6367.30231(36)	Σ–Σ	0203e–0200e	(1401)	7511.63569(36)	0.4101432(21)	2.921(28)	9.5(10)	P45/R43	67/79	1.17	
6367.30412(52)		*0203e–0200e*[L]		*7511.63750(52)*	*0.4101389(36)*	*2.823(60)*	*4.7(27)*	*P33/R38*	*37/42*	*1.0*	
6370.39732(52)	Σ–Σ	1003e–1000e	(1403)	7650.75144(52)	0.4071089(32)	1.778(38)		P27/R29	34/40	1.30	
6406.42084(31)	Π–Π	0113e–0110e	(1311)	6981.85449(31)	0.4092308(12)	1.775(11)	0.40(29)	P53/R51	68/99	0.86	
6406.42319(43)		*0113e–0110e*[L]		*6981.85684(43)*	*0.40922940(98)*	*1.7627(43)*		*P39/R49*	*62/70*	*1.7*	
6406.4211(13)		0113e–0110f		6981.8548(13)	0.409222(39)	2.4(21)		Q13	11/13	1.9	
6406.41860(36)		0113f–0110f		6981.85225(36)	0.4100011(15)	1.801(15)	0.51(41)	P51/R49	61/93	1.08	
6406.42113(39)		*0113f–0110f*[L]		*6981.85478(39)*	*0.40999680(88)*	*1.7728(37)*		*P39/R52*	*67/74*	*1.7*	
6406.4193(11)		0113f–0110e		6981.8530(11)	0.409990(29)	1.5(14)		Q14	12/13	1.9	
6757.67844(60)	Π–Π	2112e–0110f	(1317)	7333.11209(60)	0.4089083(58)	1.94(14)	14.8(88)	P34/R31	51/57	1.42	
6757.68261(79)		2112f–0110f		7333.11626(79)	0.4098220(60)	1.468(89)		P26/R24	35/40	1.55	
7039.72567(58)	Π–Π	4111e–0110e (2511e–0110e)	(13110)	7615.15932(58)	0.4106869(28)	2.052(28)		P33/R31	36/55	1.08	
7039.72457(72)		4111f–0110f (2511f–0110f)		7615.15822(72)	0.4125654(34)	2.122(36)		P31/R30	34/55	1.25	
7149.73271(40)	Π–Π	4111e–0110e	(13112)	7725.16636(40)	0.4087723(27)	1.449(42)	−2.7(1.8)	P35/R40	55/64	1.23	
7149.72916(44)		4111f–0110f		7725.16281(44)	0.4100978(49)	1.54(13)	8.0(89)	P31/R30	45/50	1.09	
7614.99969(37)	Π–Π	1113e–0110e	(1513)	8190.43334(37)	0.4073935(23)	1.633(35)	−5.0(15)	P41/R40	65/76	1.05	
7614.99970(44)		1113f–0110f		8190.43335(44)	0.4082234(17)	1.690(17)	−1.40(45)	P49/R50	78/94	1.36	

Diagonal matrix element:

$$\begin{aligned}\langle V_1V_2\ell_2V_3J|H^{\text{eff}}|V_1V_2\ell_2V_3J\rangle &= \sum_i \omega_i\Big(V_i+\frac{g_i}{2}\Big)\\ &+\sum_{ij}x_{ij}\Big(V_i+\frac{g_i}{2}\Big)\Big(V_j+\frac{g_j}{2}\Big)+x_{\ell\ell}\ell_2^2\\ &+\sum_{ijk}y_{ijk}\Big(V_i+\frac{g_i}{2}\Big)\Big(V_j+\frac{g_j}{2}\Big)\Big(V_k+\frac{g_k}{2}\Big)\\ &+\sum_i y_{i\ell\ell}\Big(V_i+\frac{g_i}{2}\Big)\ell_2^2+\sum_{ijmn}z_{ijmn}\Big(V_i+\frac{g_i}{2}\Big)\Big(V_j+\frac{g_j}{2}\Big)\\ &\times\Big(V_m+\frac{g_m}{2}\Big)\Big(V_n+\frac{g_n}{2}\Big)+\sum_{ij}z_{ij\ell\ell}\Big(V_i+\frac{g_i}{2}\Big)\Big(V_j+\frac{g_j}{2}\Big)\ell_2^2\\ &+z_{\ell\ell\ell\ell}\ell_2^4+\Bigg\{B_e-\sum_i\alpha_i\Big(V_i+\frac{g_i}{2}\Big)\\ &+\sum_{ij}\gamma_{ij}\Big(V_i+\frac{g_i}{2}\Big)\Big(V_j+\frac{g_j}{2}\Big)+\gamma_{\ell\ell}\ell_2^2\\ &+\sum_{ijk}\varepsilon_{ijk}\Big(V_i+\frac{g_i}{2}\Big)\Big(V_j+\frac{g_j}{2}\Big)\Big(V_k+\frac{g_k}{2}\Big)\\ &+\sum_i\varepsilon_{i\ell\ell}\Big(V_i+\frac{g_i}{2}\Big)\ell_2^2\Bigg\}\big[J(J+1)-\ell_2^2\big]\\ &-\Bigg\{D_e+\sum_i\beta_i\Big(V_i+\frac{g_i}{2}\Big)+\sum_{ij}\eta_{ij}\Big(V_i+\frac{g_i}{2}\Big)\Big(V_j+\frac{g_j}{2}\Big)\\ &+\eta_{\ell\ell}\ell_2^2\Bigg\}\big[J(J+1)-\ell_2^2\big]^2+\Bigg\{H_e+\sum_i\delta_i\Big(V_i+\frac{g_i}{2}\Big)\Bigg\}\\ &\times\big[J(J+1)-\ell_2^2\big]^3. \end{aligned}\tag{4}$$

ℓ-Doubling matrix element:

$$\begin{aligned}&\langle V_1V_2\ell_2V_3J|H^{\text{eff}}|V_1V_2\ell_2\pm2V_3J\rangle\\ &=\sqrt{(V_2\pm\ell_2+2)(V_2\mp\ell_2)[J(J+1)-\ell_2(\ell_2\pm1)][J(J+1)-(\ell_2\pm1)(\ell_2\pm2)]}\\ &\times\Bigg\{L_e+\sum_i L_i\Big(V_i+\frac{g_i}{2}\Big)+\sum_{ij}L_{ij}\Big(V_i+\frac{g_i}{2}\Big)\Big(V_j+\frac{g_j}{2}\Big)\\ &+L_J\Big[J(J+1)-(\ell_2\pm1)^2\Big]\Bigg\}\end{aligned}\tag{5}$$

Matrix elements of anharmonic resonance interactions:

$$\begin{aligned}\langle V_1V_2\ell_2V_3J|H^{\text{eff}}|V_1-1V_2+2\ell_2V_3J\rangle &= \sqrt{V_1(V_2+\ell_2+2)(V_2-\ell_2+2)}\\ &\times\Bigg\{F_e+\sum_i F_i\Big(V_i+\frac{g_i}{2}\Big)+\sum_{ij}F_{ij}\Big(V_i+\frac{g_i}{2}\Big)\Big(V_j+\frac{g_j}{2}\Big)\\ &+F_{\ell\ell}\ell_2^2+F_J\big[J(J+1)-\ell_2^2\big]\Bigg\},\end{aligned}\tag{6}$$

$$\begin{aligned}\langle V_1V_2\ell_2V_3J|H^{\text{eff}}|V_1-2V_2\ell_2V_3+1J\rangle &= \sqrt{(V_1-1)V_1(V_3+1)}\times\Bigg\{F_e^{(2)}+\sum_i F_i^{(2)}\Big(V_i+\frac{g_i}{2}\Big)\\ &+\sum_{ij}F_{ij}^{(2)}\Big(V_i+\frac{g_i}{2}\Big)\Big(V_j+\frac{g_j}{2}\Big)+F_{\ell\ell}^{(2)}\ell_2^2\\ &+F_J^{(2)}\big[J(J+1)-\ell_2^2\big]\Bigg\},\end{aligned}\tag{7}$$

$$\begin{aligned}\langle V_1V_2\ell_2V_3J|H^{\text{eff}}|V_1-1V_2-2\ell_2V_3+1J\rangle &= \sqrt{V_1(V_2-\ell_2)(V_2+\ell_2)(V_3+1)}\\ &\times\Bigg\{F_e^{(3)}+\sum_i F_i^{(3)}\Big(V_i+\frac{g_i}{2}\Big)\\ &+\sum_{ij}F_{ij}^{(3)}\Big(V_i+\frac{g_i}{2}\Big)\Big(V_j+\frac{g_j}{2}\Big)+F_{\ell\ell}^{(3)}\ell_2^2\\ &+F_J^{(3)}\big[J(J+1)-\ell_2^2\big]\Bigg\},\end{aligned}\tag{8}$$

$$\begin{aligned}\langle V_1V_2\ell_2V_3J|H^{\text{eff}}|V_1V_2-4\ell_2V_3+1J\rangle &= \sqrt{(V_3+1)\big(V_2^2-\ell_2^2\big)\Big[(V_2-2)^2-\ell_2^2\Big]}\\ &\times\Bigg\{F_e^{(4)}+\sum_i F_i^{(4)}\Big(V_i+\frac{g_i}{2}\Big)+F_J^{(4)}\big[J(J+1)-\ell_2^2\big]\Bigg\},\end{aligned}\tag{9}$$

$$\begin{aligned}\langle V_1V_2\ell_2V_3J|H^{\text{eff}}|V_1-2V_2+4\ell_2V_3J\rangle &= \sqrt{V_1(V_1-1)(V_2+\ell_2+2)(V_2+\ell_2+4)(V_2-\ell_2+2)(V_2-\ell_2+4)}\\ &\times\Bigg\{F_e^{(5)}+\sum_i F_i^{(5)}\Big(V_i+\frac{g_i}{2}\Big)+F_J^{(5)}\big[J(J+1)-\ell_2^2\big]\Bigg\},\end{aligned}\tag{10}$$

$$\begin{aligned}\langle V_1V_2\ell_2V_3J|H^{\text{eff}}|V_1-3V_2+2\ell_2V_3+1J\rangle &= \sqrt{(V_1-3)(V_1-2)(V_1-1)(V_2+2-\ell_2)(V_2+2+\ell_2)(V_3+1)}\\ &\times\Bigg\{F_e^{(7)}+\sum_i F_i^{(7)}\Big(V_i+\frac{g_i}{2}\Big)+F_J^{(7)}\big[J(J+1)-\ell_2^2\big]\Bigg\},\end{aligned}\tag{11}$$

$$\begin{aligned}\langle V_1V_2\ell_2V_3J|H^{\text{eff}}|V_1+1V_2-6\ell_2V_3+1J\rangle &= \sqrt{(V_1+1)(V_3+1)\big(V_2^2-\ell_2^2\big)\Big[(V_2-2)^2-\ell_2^2\Big]\Big[(V_2-4)^2-\ell_2^2\Big]}\\ &\times\Bigg\{F_e^{(10)}+\sum_i F_i^{(10)}\Big(V_i+\frac{g_i}{2}\Big)+F_J^{(10)}\big[J(J+1)-\ell_2^2\big]\Bigg\},\end{aligned}\tag{12}$$

Matrix elements of anharmonic + ℓ-type resonance interactions:

$$\langle V_1V_2\ell_2V_3J|H^{\text{eff}}|V_1-1V_2+2\ell_2\pm2V_3J\rangle = F_e^L\sqrt{V_1(V_2\pm\ell_2+2)(V_2\pm\ell_2+4)[J(J+1)-\ell_2(\ell_2\pm1)][J(J+1)-(\ell_2\pm1)(\ell_2\pm2)]}, \quad (13)$$

$$\langle V_1V_2\ell_2V_3J|H^{\text{eff}}|V_1-1V_2-2\ell_2\pm2V_3+1J\rangle = F_e^{(3)L}\sqrt{V_1(V_3+1)(V_2\mp\ell_2)(V_2\mp\ell_2-2)[J(J+1)-\ell_2(\ell_2\pm1)][J(J+1)-(\ell_2\pm1)(\ell_2\pm2)]}, \quad (14)$$

$$\langle V_1V_2\ell_2V_3J|H^{\text{eff}}|V_1V_2-4\ell_2\pm2V_3+1J\rangle = F_e^{(4)L}\sqrt{(V_3+1)\left(V_2^2-\ell_2^2\right)(V_2\mp\ell_2-2)(V_2\mp\ell_2-4)[J(J+1)-\ell_2(\ell_2\pm1)][J(J+1)-(\ell_2\pm1)(\ell_2\pm2)]}. \quad (15)$$

In the Eqs. (4) and (5) g_i is the degeneracy of the vibrational mode i: $g_i=1$ for $i=1$, 3 and $g_i=2$ for $i=2$. In the Eqs. (6)–(12) $g_i=g_i'+\Delta V_i$, where g_i' is the degeneracy of the vibrational mode i and ΔV_i define matrix element $\langle V_1V_2\ell_2V_3J \mid H^{\text{eff}} \mid V_1+\Delta V_1V_2+\Delta V_2\ell_2V_3+\Delta V_3J\rangle$.

5. Least-squares fittings

The parameters of the above presented effective Hamiltonian have been fitted to the available experimental line positions collected from this work and other measurements reported in Refs. [1–13,22]. The measurements include microwave, Fourier-transform, ICLAS and CRDS. The stated accuracies of the measurements range from 6.6×10^{-7} to 5×10^{-3} cm^{-1}. Note that the line positions from Toth's web site [22] are mostly calculated values. In the case of unperturbed bands they were calculated using spectroscopic parameters. For the perturbed bands the observed line positions are given there. Taking this into account, we used 10^{-3} cm^{-1} as the experimental uncertainty for these data. Finally the data used in our fitting comprises nearly 18 000 line positions and covers the spectral region 0–8857 cm^{-1}.

The data was then checked for the internal consistency. The misassigned, misprinted or improperly measured lines were revealed. This checking was done by fitting energy levels to the observed line positions using the fundamental Ritz principle. Details of this approach can be found in Ref. [23]. The following criterion for deleting a line from the fit was applied: If the weighted Ritz residual

$$r_{i\to j}=\frac{\nu_{i\to j}^{\text{obs}}-(E_i-E_j)}{\delta_{i\to j}^{\text{obs}}} \quad (16)$$

of a line is greater than 3, then the line will be deleted from the data. In the above equation, $\nu_{i\to j}^{\text{obs}}$ and $\delta_{i\to j}^{\text{obs}}$ are observed line position and its experimental uncertainty of a transition between an upper state i and a lower state j, and E_i

Table 4
Spectrum-by-spectrum analysis of the experimental data and statistics of the line positions fit for $^{14}N^{15}N^{16}O$

Reference	Type of the spectrum	Calibration factor	Accuracy (in 10^{-3} cm^{-1})	N_{fit}	Spectral range (in cm^{-1})	RMS$_{Ritz}$ (in 10^{-3} cm^{-1})	RMS1 (in 10^{-3} cm^{-1})	RMS2 (in 10^{-3} cm^{-1})
Morino et al. [2]	MW	1.000000000	0.00066	3	20.9–22.6	0.00002	0.0022	0.0025
Andreev et al. [1]	MW	1.000000000	0.0017	22	12.6–18.5	0.00007	0.0023	0.0031
Drouin et al. [3]	MW	1.000000000	0.003	8	28.5–54.3	0.0004	0.0096	0.0091
Toth [8]	FTS	1.000000000	0.06	273	2386.8–3463.5	0.06	0.15	0.15
Toth [7]	FTS	1.000000000	0.06	254	1102.7–2216.5	0.04	0.08	0.08
Guelachvili [6]	FTS	0.999999824	0.13	115	1223.7–1324.3	0.09	0.04	0.06
This work	FTS	1.000000000	1.0	11017	3496.1–8857.1	0.6	1.47	1.56
Toth [22]	FTS	1.000000000	1.0	2430	529.8–5085.7	0.2	1.15	1.28
Herbin et al. [11]	ICLAS	1.000000000	1.0	138	3910.7–4021.6	0.7	1.15	1.04
Liu et al. [12,13]	CRDS	1.000000000	2.0	760	5906.4–6791.7	1.5	1.89	1.90
Wang et al. [10]	FTS	1.000000000	2.0	45	6402.6–6462.9	1.8	2.38	1.96
Amiot [5]	FTS	0.999999983	2.0	995	3582.7–5553.1	0.9	1.03	1.11
Krell and Sams [4]	FTS	1.000000402	5.0	80	2391.6–2578.2	1.6	1.64	1.64

Table 5
Fit summary

P_1	P_2	Band		J_{max}	N_{lin}	FIT1	$\chi = 1.38$	FIT2	$\chi = 1.46$	Refs.		
						RMS[a]	MRES	RMS	MRES			
0	0	00001	00001	65	19	0.01	0.00	0.01	0.00	[1]	[2]	[3]
1	0	01101	00001	60	114	0.32	0.19	0.50	0.41	[22]		
1	0	01102	00001	60	60	0.23	0.12	0.86	0.59	[22]		
1	1	01101	01101	22	6	0.00	0.00	0.00	0.00	[1]		
1	1	01102	01102	22	8	0.00	0.00	0.00	0.00	[1]		
2	0	02001	00001	50	53	0.11	0.00	0.11	−0.02	[7]		
2	0	10001	00001	70	198	0.06	−0.01	0.07	−0.01	[6]	[7]	
2	1	02201	01101	45	80	3.24	−2.13	4.15	−3.03	[22]		
2	1	02201	01102	46	45	3.28	−1.83	4.13	−2.89	[22]		
2	1	02202	01101	46	45	2.05	1.62	1.08	0.74	[22]		
2	1	02202	01102	45	80	1.77	1.42	0.84	0.61	[22]		
3	0	11101	00001	40	66	0.57	0.55	0.68	0.68	[22]		
3	0	11102	00001	40	40	0.94	0.86	1.35	1.27	[22]		
3	1	11101	01101	59	110	0.51	0.44	0.49	0.18	[22]		
3	1	11101	01102	18	18	0.50	0.49	0.65	0.65	[22]		
3	1	11102	01101	18	18	0.58	0.57	0.77	0.77	[22]		
3	1	11102	01102	59	115	0.99	0.56	1.09	0.91	[22]		
4	0	00011	00001	75	118	0.06	0.00	0.06	0.00	[7]		
4	0	04001	00001	32	54	0.68	0.15	0.62	0.52	[22]		
4	0	12001	00001	50	88	1.14	0.30	1.14	0.30	[4]	[8]	
4	0	20001	00001	62	148	0.84	−0.14	0.84	−0.14	[4]	[8]	
4	2	12201	02201	44	79	1.12	0.82	1.33	1.17	[22]		
4	2	12202	02202	44	83	0.86	0.21	0.76	0.48	[22]		
5	0	01111	00001	46	89	0.47	−0.46	0.40	−0.27	[22]		
5	0	01112	00001	48	48	0.36	−0.06	0.39	−0.20	[22]		
5	1	01111	01101	66	103	0.58	−0.57	0.55	−0.40	[22]		
5	1	01111	01102	30	30	0.47	−0.47	0.57	−0.57	[22]		
5	1	01112	01101	30	30	0.32	−0.29	0.60	−0.60	[22]		
5	1	01112	01102	66	103	0.38	−0.19	0.63	−0.59	[22]		
5	1	13101	01101	36	66	1.34	0.39	1.96	1.25	[22]		
5	1	13102	01102	37	67	0.61	−0.44	0.55	0.36	[22]		
5	1	21101	01101	48	94	0.56	0.53	0.66	−0.42	[22]		
5	1	21101	01102	3	3	0.30	0.30	0.27	0.27	[22]		
5	1	21102	01101	3	3	0.14	0.14	0.12	0.12	[22]		
5	1	21102	01102	48	93	0.47	0.40	0.24	0.00	[22]		
6	0	02011	00001	48	46	0.21	0.01	0.21	0.02	[8]		
6	0	10011	00001	61	69	0.12	0.01	0.12	0.01	[8]		
6	0	22001	00001	58	120	0.76	−0.65	1.17	−0.90	[5]	TW[b]	
6	0	14001	00001	71	223	0.54	0.35	0.69	−0.52	[5]	TW	
6	0	30001	00001	74	220	1.46	−1.17	1.42	−1.18	[5]	TW	
6	2	02211	02201	54	77	1.73	−0.21	2.05	0.20	[22]		
6	2	02211	02202	20	19	1.38	−1.20	1.24	−1.04	[22]		
6	2	02212	02201	20	19	0.58	−0.25	0.56	−0.07	[22]		
6	2	02212	02202	54	77	2.09	−1.74	1.60	−1.37	[22]		
7	0	03111	00001	44	49	1.29	−1.01	0.82	0.12	TW		
7	0	03112	00001	45	21	0.77	0.22	1.06	0.74	TW		
7	0	11111	00001	65	201	0.80	−0.49	0.97	0.25	[5]	[11]	TW
7	0	11112	00001	62	100	0.91	−0.10	0.76	0.11	[11]	TW	
7	0	15101	00001	40	22	1.32	−0.70	1.23	−0.21	TW		
7	0	15102	00001	36	19	0.69	−0.21	0.90	0.47	TW		
7	0	31101	00001	51	64	1.30	0.48	1.41	0.54	TW		
7	0	31102	00001	46	41	0.67	−0.36	0.63	0.15	TW		
7	1	03111	01101	26	35	0.63	−0.59	0.47	0.43	[22]		
7	1	03112	01102	26	36	0.40	0.38	1.12	1.09	[22]		
7	1	11111	01101	50	95	0.73	−0.69	0.37	−0.32	[22]		
7	1	11111	01102	5	5	1.07	−1.07	0.64	−0.64	[22]		
7	1	11112	01101	5	5	1.01	−1.01	0.59	−0.59	22		

[a] RMS and MRES are in units of 10^{-3} cm^{-1}.
[b] TW - this work.

(*continued on next page*)

Table 5 (*continued*)

P_1	P_2	Band		J_{max}	N_{lin}	FIT1	$\chi = 1.38$	FIT2	$\chi = 1.46$	Refs.		
						RMS[a]	MRES	RMS	MRES			
7	1	11112	01102	50	97	0.58	−0.32	0.54	−0.44	[22]		
7	1	15101	01101	63	144	0.53	−0.38	0.56	0.03	[5]	TW	
7	1	15102	01102	65	154	0.71	−0.60	0.87	0.20	[5]	TW	
7	1	23101	01101	55	89	0.66	0.27	1.23	1.00	TW		
7	1	23102	01102	53	89	0.67	0.30	0.52	0.18	TW		
7	1	31101	01101	67	134	0.95	−0.09	1.41	−0.40	[5]	TW	
7	1	31101	01102	23	17	1.64	−0.13	1.46	0.44	TW		
7	1	31102	01101	27	16	0.82	−0.56	0.58	0.12	TW		
7	1	31102	01102	71	173	0.91	−0.29	0.82	−0.37	[5]	TW	
8	0	00021	00001	79	340	1.01	0.51	0.80	−0.15	[22]	[5]	TW
8	0	04011	00001	54	92	1.75	−0.95	1.86	−1.37	TW		
8	0	12011	00001	67	174	0.88	−0.04	0.56	0.03	[5]	TW	
8	0	16001	00001	45	139	0.92	0.12	1.06	0.02	[5]	TW	
8	0	20011	00001	76	225	0.80	0.26	0.82	0.30	[5]	TW	
8	0	08001	00001	62	108	1.05	−0.01	1.25	−0.65	TW		
8	0	24001	00001	57	107	0.80	0.76	0.36	−0.15	TW		
8	0	40001	00001	64	195	1.31	−0.76	1.28	−0.78	[5]	[22]	TW
8	1	00021	01101	47	50	1.60	0.01	1.72	−0.79	TW		
8	1	00021	01102	37	22	1.01	0.26	1.07	−0.62	TW		
8	1	12011	01101	55	131	0.98	0.23	0.99	−0.02	[11]	TW	
8	1	12011	01102	43	45	0.77	0.07	0.91	−0.23	[11]	TW	
8	1	12211	01101	48	78	0.66	0.20	0.63	0.18	TW		
8	1	12211	01102	44	40	0.65	0.18	0.62	0.12	TW		
8	1	12212	01101	49	45	1.28	−0.41	1.00	−0.25	TW		
8	1	12212	01102	53	83	0.82	0.04	0.68	0.12	TW		
8	1	20011	01101	42	68	0.68	−0.40	0.78	−0.55	TW		
8	1	20011	01102	46	44	0.56	−0.23	0.67	−0.42	TW		
8	2	16001	02001	51	77	0.61	−0.46	0.99	−0.58	TW		
8	2	16001	10001	49	79	0.51	−0.37	0.95	−0.54	TW		
8	2	16201	02201	51	65	1.72	−0.95	2.36	−1.16	TW		
8	2	16202	02202	49	70	1.18	−0.33	1.78	−0.53	TW		
8	2	20011	02001	35	58	1.24	−0.93	1.21	−0.87	TW		
8	2	20011	10001	37	68	0.47	−0.39	0.47	−0.37	[22]		
8	2	24001	02001	53	6	0.78	−0.52	1.95	−1.87	TW		
8	2	32001	02001	53	79	0.67	−0.23	1.29	−1.08	TW		
8	2	32001	10001	47	35	1.57	−0.79	2.09	−1.65	TW		
8	2	32201	02201	50	67	1.01	−0.63	1.38	−1.10	TW		
8	2	32202	02202	50	75	1.70	−1.44	2.01	−1.75	TW		
8	2	40001	02001	46	70	1.63	−1.45	1.64	−1.41	TW		
8	2	40001	10001	52	89	1.36	−1.33	1.41	−1.36	TW		
9	0	01121	00001	59	110	1.61	1.44	1.28	1.01	TW		
9	0	01122	00001	59	73	1.38	1.00	1.45	0.79	[5]	TW	
9	0	21111	00001	38	34	1.20	−0.21	1.29	−0.65	TW		
9	0	21112	00001	30	23	1.13	−0.88	1.43	−1.24	TW		
9	1	01121	01101	72	191	0.76	0.22	0.77	−0.45	[5]	[22]	TW
9	1	01121	01102	25	15	0.84	0.62	0.58	−0.07	TW		
9	1	01122	01101	31	19	1.08	0.85	0.74	0.14	TW		
9	1	01122	01102	72	192	0.73	0.24	0.81	−0.33	[5]	[22]	TW
9	1	05111	01101	42	65	1.03	0.44	0.94	0.53	TW		
9	1	05112	01102	30	52	0.72	0.01	0.80	−0.21	TW		
9	1	13111	01101	56	98	0.54	−0.09	0.44	0.35	TW		
9	1	13112	01102	55	98	0.71	0.64	0.59	0.55	TW		
9	1	21111	01101	61	153	1.05	−0.43	1.47	−0.86	[5]	TW	
9	1	21112	01102	62	153	0.93	−0.37	1.33	−1.00	[5]	TW	
9	1	25101	01101	51	90	0.38	0.20	1.59	1.52	TW		
9	1	25102	01102	46	80	0.34	−0.08	0.81	0.71	TW		
9	1	33101	01101	48	76	1.47	1.29	1.50	1.17	TW		
9	1	33102	01102	53	88	0.92	0.67	1.23	0.80	TW		
9	1	41101	01101	53	88	0.83	0.15	1.11	0.50	TW		
9	1	41102	01102	54	97	0.51	0.01	1.14	0.91	TW		
9	2	21111	10001	36	34	1.60	−0.11	1.63	−0.60	TW		
9	2	21112	10001	35	31	1.25	−0.39	1.44	−0.83	TW		
9	3	41101	11101	41	47	1.34	−1.05	1.01	−0.51	TW		
9	3	41102	11102	44	43	0.88	−0.49	0.90	0.17	TW		

Table 5 (*continued*)

P_1	P_2	Band		J_{max}	N_{lin}	FIT1	$\chi = 1.38$	FIT2	$\chi = 1.46$	Refs.		
						RMS[a]	MRES	RMS	MRES			
10	0	02021	00001	45	81	0.70	−0.39	0.92	−0.73	TW		
10	0	10021	00001	63	121	0.63	0.09	0.52	0.26	[5]	TW	
10	0	06011	00001	54	85	1.23	−0.54	1.64	0.31	TW		
10	0	22011	00001	51	100	1.05	0.45	1.14	−0.08	TW		
10	0	26001	00001	51	169	1.17	−0.05	1.44	0.46	[12]	TW	
10	0	30011	00001	60	161	1.92	−1.44	1.41	−0.71	[13]	TW	
10	0	34001	00001	34	50	1.75	−0.98	2.21	−0.68	TW		
10	0	42001	00001	49	145	1.38	−0.22	1.53	−0.29	[13]	TW	
10	0	50001	00001	56	174	1.24	0.83	1.10	0.43	[12]	TW	
10	1	02021	01101	48	77	0.83	0.17	0.84	−0.36	TW		
10	1	02021	01102	43	37	0.64	0.40	0.50	−0.17	TW		
10	1	02221	01101	43	69	1.11	0.72	0.94	0.59	TW		
10	1	02221	01102	39	34	1.06	0.76	0.90	0.59	TW		
10	1	02222	01101	45	38	0.95	0.23	0.85	−0.01	TW		
10	1	02222	01102	45	71	1.23	0.58	1.13	0.32	TW		
10	2	02021	02001	57	103	0.91	−0.62	1.19	−0.97	TW		
10	2	02221	02201	21	36	0.75	0.06	0.74	0.20	TW		
10	2	02222	02202	27	42	1.06	0.38	1.19	0.56	TW		
10	2	10021	10001	55	89	0.50	0.07	0.58	0.38	TW		
10	2	06011	02001	46	76	1.27	−0.23	1.84	0.78	TW		
10	2	14211	02201	50	79	1.03	−0.20	1.71	−1.32	TW		
10	2	14212	02202	50	82	1.44	1.07	1.14	−0.01	TW		
10	2	22011	02001	49	77	0.95	0.58	0.94	0.10	TW		
10	2	22011	10001	42	64	1.04	0.69	0.90	0.20	TW		
10	2	22211	02201	32	42	1.47	−1.00	1.23	0.60	TW		
10	2	22212	02202	32	42	1.79	−1.49	1.25	0.02	TW		
10	2	26001	02001	37	43	1.01	0.03	1.19	0.51	TW		
10	2	26001	10001	44	69	1.35	1.07	1.61	1.40	TW		
10	2	30011	10001	55	96	0.86	−0.78	0.35	−0.05	TW		
10	2	34201	02201	36	55	2.73	2.44	2.25	1.92	TW		
10	2	42001	02001	38	56	1.79	1.42	1.85	1.42	TW		
10	2	42201	02201	39	44	1.82	−0.94	2.04	−0.58	TW		
10	2	42202	02202	28	34	1.63	0.63	1.76	0.68	TW		
10	2	50001	10001	43	74	2.58	2.48	2.27	2.16	TW		
11	0	11121	00001	39	58	1.47	−1.02	1.14	−0.38	TW		
11	0	11122	00001	37	33	0.92	−0.34	0.90	−0.06	TW		
11	1	03121	01101	24	33	1.35	0.67	1.21	−0.07	TW		
11	1	03122	01102	36	51	1.42	0.72	1.76	0.87	TW		
11	1	11121	01101	45	71	1.02	0.45	1.18	0.80	TW		
11	1	11122	01102	45	77	1.53	1.12	1.66	0.99	TW		
11	1	15111	01101	44	76	1.48	−0.20	1.76	−1.08	TW		
11	1	15112	01102	44	74	1.05	−0.54	0.89	0.01	TW		
11	1	27101	01101	34	26	1.23	−0.05	1.40	−0.15	TW		
11	1	31111	01101	52	93	1.95	1.34	1.64	0.90	[13]	TW	
11	1	31112	01102	50	105	1.36	0.42	1.83	0.87	[13]	TW	
11	1	35101	01101	34	44	1.22	−0.23	1.37	−0.24	TW		
11	1	35102	01102	33	42	1.34	−0.12	1.70	−0.29	TW		
11	1	43101	01101	43	60	1.89	−1.67	2.44	−1.78	TW		
11	1	43102	01102	41	66	1.54	0.81	1.07	0.43	TW		
11	1	51101	01101	42	101	1.63	0.55	1.54	0.55	[13]	TW	
11	1	51102	01102	43	100	1.44	0.40	1.55	−0.78	[13]	TW	
11	2	03321	02201	21	25	1.86	0.59	2.45	1.80	TW		
11	2	03321	02202	40	27	1.44	−0.90	1.71	−0.62	TW		
11	2	03322	02201	42	30	1.28	−0.39	1.93	−0.19	TW		
12	0	00031	00001	66	266	1.70	−1.21	1.29	0.56	[10]	[12]	TW
12	0	0(12)001	00001	3	5	1.10	−0.26	1.91	1.58	TW		
12	0	12021	00001	42	123	1.74	−0.82	1.65	−0.91	[12]	TW	
12	0	16011	00001	46	74	0.70	−0.60	1.09	−0.03	TW		
12	0	20021	00001	49	160	1.42	0.64	1.63	0.31	[12]	TW	
12	0	24011	00001	49	13	1.42	−0.60	2.40	−1.83	TW		
12	0	32011	00001	33	52	1.38	−0.06	2.01	0.59	TW		
12	0	40011	00001	53	99	1.86	0.11	1.49	−0.15	TW		

(*continued on next page*)

Table 5 (*continued*)

P_1	P_2	Band		J_{max}	N_{lin}	FIT1	$\chi = 1.38$	FIT2	$\chi = 1.46$	Refs.	
						RMS[a]	MRES	RMS	MRES		
12	0	52001	00001	40	73	1.43	−0.65	1.93	−0.40	TW	
12	0	60001	00001	47	85	1.22	−0.36	1.45	−0.36	TW	
12	2	12021	02001	29	46	1.42	0.88	1.27	0.66	TW	
12	2	12221	02201	27	37	1.57	−0.37	2.26	−1.59	TW	
12	2	20021	10001	41	64	1.29	0.72	1.52	0.43	TW	
12	2	32211	02201	32	39	2.64	2.05	2.83	2.05	TW	
12	2	40011	10001	36	53	2.29	2.01	1.87	1.50	TW	
13	0	01131	00001	31	27	2.17	−1.49	1.85	−0.82	TW	
13	0	01132	00001	29	25	1.96	−1.48	1.48	−0.62	TW	
13	1	01131	01101	52	122	1.66	0.17	1.61	0.49	[12]	TW
13	1	01131	01102	13	14	2.10	−1.16	1.93	−0.87	[12]	TW
13	1	01132	01101	14	12	2.66	−2.43	2.34	−2.09	[12]	TW
13	1	01132	01102	53	122	1.99	−0.45	2.47	0.75	[12]	TW
13	1	21121	01101	33	47	1.96	−1.05	1.81	−0.94	TW	
13	1	21122	01102	25	31	1.46	−0.78	1.50	−0.84	TW	
13	1	33111	01101	41	51	1.45	−0.16	1.82	−0.65	TW	
13	1	33112	01102	31	44	2.17	−1.64	1.79	−1.05	TW	
13	1	41111	01101	32	48	2.06	0.98	1.77	0.53	TW	
13	1	41112	01102	30	44	2.16	−0.79	2.14	−0.89	TW	
14	0	02031	00001	43	73	1.63	0.67	1.78	0.87	TW	
14	0	10031	00001	57	109	0.79	−0.31	0.57	−0.30	TW	
14	0	22021	00001	32	56	1.47	0.08	1.74	0.69	TW	
14	0	26011	00001	30	28	14.19	4.98	13.39	4.55	TW	
14	0	30021	00001	44	80	0.98	−0.03	1.00	−0.23	TW	
14	0	34011	00001	21	16	9.20	−8.76	8.15	−7.73	TW	
14	0	50011	00001	34	52	2.21	−0.39	5.51	−0.30	TW	
14	2	02031	02001	43	105	1.52	−0.22	1.47	0.09	[13]	TW
14	2	02231	02201	26	73	1.50	0.16	1.54	−0.52	[13]	TW
14	2	02232	02202	35	8	3.40	−1.92	2.87	−1.32	TW	
14	2	10031	10001	30	33	1.62	−1.00	1.91	−1.24	TW	
15	1	11131	01101	41	62	0.90	0.09	1.03	0.24	TW	
15	1	11132	01102	51	78	1.69	0.73	1.87	0.41	TW	
16	0	00041	00001	55	92	2.01	1.23	2.16	0.00	TW	
16	0	20031	00001	41	62	1.01	−0.05	1.26	0.25	TW	

and E_j are corresponding Ritz energies (term values). Old measurements [4–6] were calibrated against more recent measurements. The deletion criterion enabled us to exclude nearly 1500 lines. The weighted standard deviation of the revised data pool was 0.73. The RMS of residuals was 0.00084 cm^{-1}. These numbers give a quantitative measurement of the internal consistency of the observed data. The summary of the Ritz fit is given in Table 4. It is shown that the stated accuracy of each measurement is confirmed by the Ritz fit of the revised data. In particular, the actual average accuracy of the measurements performed in the present work is about 0.0006 cm^{-1}.

The revised data was then compiled as an input file used for the least-squares fittings of the effective Hamiltonian parameters. The fittings have been performed using GIP computer code [24]. It minimizes the dimensionless weighted standard deviation which is defined as:

$$\chi = \sqrt{\frac{\sum_i \left[(\nu_i^{obs} - \nu_i^{calc})/\varepsilon^k\right]^2}{N-n}}, \tag{17}$$

where ν_i^{obs} and ν_i^{calc} are the observed and calculated wavenumbers, N is the number of fitted transitions and n is the number of adjusted parameters, and ε^k is the experimental uncertainty of the spectrum (index k). To give additional characteristics of the quality of the fit we also use the root mean squares (RMS) of the residuals which is defined as

$$\mathrm{RMS} = \sqrt{\frac{1}{N}\sum_i (\nu_i^{obs} - \nu_i^{calc})^2}. \tag{18}$$

The input data were weighted according to their experimental uncertainties ε^k. It is well known that due to the nonlinear dependence of the eigenvalues of the effective Hamiltonian matrix on the matrix elements, the fitted sum of squares of the residuals has many minima [25]. Several sets of parameters were found which could reproduce the input observed data with approximately the same quality. In order to choose the best set we have to analyze the values of the fitted parameters. Their values must agree with orders of the perturbation theory. Moreover the fitting itself is a very time consuming process since one has to try many sets of parameters to obtain a good standard deviation of the fit. Finally two sets of parameters were chosen as solutions. They will be referenced as set 1 and set 2. In order to avoid 100% correlations, diagonal vibrational parameter $x_{\ell\ell}$ in both fits was fixed to the value given

Table 6
The effective Hamiltonian parameters for $^{14}N^{15}N^{16}O$

N	Parameter	Value (cm^{-1})		Order	N	Parameter	Value (cm^{-1})		Order
		Fit 1	Fit 2				Fit 1	Fit 2	
Diagonal vibrational parameters									
1	ω_1	1296.8254(18)[a]	1297.1031(46)		22	$y_{2\ell\ell}$	1.9992(85)	0.880(46)	10^{-2}
2	ω_2	582.6831(11)	582.7742(23)		23	$y_{3\ell\ell}$	−3.75(18)	−3.41(13)	10^{-2}
3	ω_3	2232.8228(20)	2232.6051(32)		24	z_{1111}	−13.26(17)	−33.76(70)	10^{-4}
4	x_{11}	−4.4515(27)	−5.190(17)		25	z_{1112}	−11.6(17)	−57.9(12)	10^{-4}
5	x_{12}	−5.2364(14)	−5.2620(17)		26	z_{1113}	97.7(34)	−136.2(61)	10^{-4}
6	x_{13}	−25.188(12)	−22.253(68)		27	z_{1122}		−117.3(21)	10^{-4}
7	x_{22}	1.04505(42)	1.03720(50)		28	z_{1123}	−319(11)	793.4(93)	10^{-4}
8	x_{23}	−13.80643(68)	−13.75245(93)		29	z_{1133}	−399.4(97)	781(16)	10^{-4}
9	x_{33}	−14.41261(25)	−14.3393(11)		30	z_{1222}	−3.17(40)	−16.3(11)	10^{-4}
10	$x_{\ell\ell}$[b]	−0.537788826	−0.537788826		31	z_{1223}	−31.0(50)	256.7(86)	10^{-4}
11	y_{111}	−2.548(61)	9.85(16)	10^{-2}	32	z_{1233}	289(12)		10^{-4}
12	y_{112}		10.01(21)	10^{-2}	33	z_{1333}	28.33(90)	76.7(25)	10^{-4}
13	y_{113}	−8.21(30)	−79.66(93)	10^{-2}	34	z_{2222}	−1.311(32)	−1.401(76)	10^{-4}
14	y_{122}	−0.698(55)	−8.77(35)	10^{-2}	35	z_{2223}		5.1(15)	10^{-4}
15	y_{123}	34.45(50)		10^{-2}	36	z_{2333}		17.97(59)	10^{-4}
16	y_{133}	11.40(10)	3.42(44)	10^{-2}	37	z_{3333}		12.91(31)	10^{-4}
17	y_{222}	−2.0436(75)	−0.870(52)	10^{-2}	38	$z_{11\ell\ell}$		29.4(15)	10^{-4}
18	y_{223}	8.47(18)	8.49(12)	10^{-2}	39	$z_{12\ell\ell}$		27.9(11)	10^{-4}
19	y_{233}	−1.218(11)	−2.324(36)	10^{-2}	40	$z_{13\ell\ell}$		133.3(58)	10^{-4}
20	y_{333}		−1.320(31)	10^{-2}	41	$z_{23\ell\ell}$		−16.1(17)	10^{-4}
21	$y_{1\ell\ell}$	4.478(75)	7.08(16)	10^{-2}					
Diagonal rotational and vibrational-rotational parameters									
42	B_e	0.42107432(15)	0.42106961(25)		59	ε_{222}	−0.3446(49)	−0.2287(41)	10^{-6}
43	α_1	1.916076(96)	1.91536(14)	10^{-3}	60	ε_{223}	1.985(43)	1.531(24)	10^{-6}
44	α_2	−0.54229(15)	−0.54381(12)	10^{-3}	61	ε_{233}	−0.201(31)		10^{-6}
45	α_3	3.34919(12)	3.348153(91)	10^{-3}	62	ε_{1LL}	0.683(44)		10^{-6}
46	γ_{11}	−0.921(11)	−1.209(19)	10^{-5}	63	ε_{2LL}	−0.449(30)		10^{-6}
47	γ_{12}	−0.666(34)	0.429(60)	10^{-5}	64	ε_{3LL}	−0.414(42)		10^{-6}
48	γ_{13}	−0.793(35)	−0.380(68)	10^{-5}	65	D_e	0.173149(18)	0.173071(19)	10^{-6}
49	γ_{22}	−1.005(11)	−1.258(15)	10^{-5}	66	β_1	1.910(13)	1.795(16)	10^{-9}
50	γ_{23}	3.025(13)	2.9577(76)	10^{-5}	67	β_2	2.615(20)	2.680(20)	10^{-9}
51	γ_{33}	−0.4605(42)	−0.5177(27)	10^{-5}	68	β_3	−0.789(16)	−0.612(11)	10^{-9}
52	$\gamma_{\ell\ell}$	0.6347(90)	0.754(15)	10^{-5}	69	η_{11}	7.49(56)	4.74(60)	10^{-11}
53	ε_{111}		0.187(11)	10^{-6}	70	η_{12}	−40.0(14)	−34.3(19)	10^{-11}
54	ε_{112}		0.572(41)	10^{-6}	71	η_{13}		−8.0(10)	10^{-11}
55	ε_{113}	−4.032(50)	−3.633(74)	10^{-6}	72	η_{22}	12.28(46)	10.08(54)	10^{-11}
56	ε_{122}	0.726(36)		10^{-6}	73	η_{23}	−20.4(11)	−14.14(94)	10^{-11}
57	ε_{123}	1.00(19)		10^{-6}	74	η_{33}	10.86(70)		10^{-11}
58	ε_{133}	1.570(36)	1.726(53)	10^{-6}					
Parameters of ℓ-doubling matrix element									
75	L_e	−0.201989(49)	−0.201311(34)	10^{-3}	81	L_{13}	−161(18)		10^{-8}
76	L_1	1.30(37)	1.57(15)	10^{-6}	82	L_{22}	−6.41(47)	−8.21(27)	10^{-8}
77	L_2	−1.460(84)	−1.888(47)	10^{-6}	83	L_{23}	89.0(38)	101.8(17)	10^{-8}
78	L_3	3.542(40)	2.799(23)	10^{-6}	84	L_{33}	−18.00(91)		10^{-8}
79	L_{11}	−61.4(66)	20.8(31)	10^{-8}	85	L_J	2.183(74)	2.532(76)	10^{-10}
80	L_{12}		−33.2(21)	10^{-8}					
Parameters of Fermi-interaction matrix element $\langle V_1V_2\ell_2V_3J\|H^{eff}\|V_1-1V_2+2\ell_2V_3J\rangle$									
86	F_e	18.94541(74)	18.94364(87)		92	F_{13}	−4.12(11)	−8.46(11)	10^{-2}
87	F_1	−0.3110(11)	−0.1696(28)		93	F_{22}		−0.423(11)	10^{-2}
88	F_2	−0.30951(24)	−0.2699(18)		94	F_{23}		1.324(71)	10^{-2}
89	F_3	−0.0570(54)	−0.3844(63)		95	F_{33}	−0.677(74)	1.914(34)	10^{-2}
90	F_{11}	0.191(17)		10^{-2}	96	F_{LL}	0.1633(20)	0.4350(51)	10^{-2}
91	F_{12}	0.2547(88)	0.629(37)	10^{-2}	97	F_J	−0.12457(27)	−0.13252(50)	10^{-3}
Parameters of Fermi-interaction matrix element $\langle V_1V_2\ell_2V_3J\|H^{\mathrm{eff}}\|V_1-2V_2\ell_2V_3+1J\rangle$									
98	$F_e^{(2)}$	−4.758(99)	17.12(18)		104	$F_{13}^{(2)}$	24.07(16)	10.40(22)	10^{-2}
99	$F_1^{(2)}$	−1.0424(45)	−0.8754(95)		105	$F_{22}^{(2)}$	4.26(13)	4.678(87)	10^{-2}
100	$F_2^{(2)}$	−0.488(25)	−1.169(17)		106	$F_{23}^{(2)}$	18.22(30)	1.13(13)	10^{-2}

(*continued on next page*)

Table 6 (*continued*)

N	Parameter	Value (cm^{-1})		Order	N	Parameter	Value (cm^{-1})		Order
		Fit 1	Fit 2				Fit 1	Fit 2	
101	$F_2^{(2)}$		−0.537(14)		107	$F_{\ell\ell}^{(2)}$		2.22(73)	10^{-2}
102	$F_{11}^{(2)}$		2.284(60)	10^{-2}	108	$F_J^{(2)}$	3.20(19)	−0.66(20)	10^{-5}
103	$F_{12}^{(2)}$	4.72(20)		10^{-2}					
Parameters of anharmonic interaction matrix element $\langle V_1V_2\ell_2V_3J\|H^{\text{eff}}\|V_1-1V_2-2\ell_2V_3+1J\rangle$									
109	$F_e^{(3)}$	−1.999(58)	−0.953(28)		115	$F_{13}^{(3)}$	2.51(18)		10^{-2}
110	$F_1^{(3)}$		−0.1925(27)		116	$F_{22}^{(3)}$	0.490(14)	0.4600(83)	10^{-2}
111	$F_2^{(3)}$	−0.1260(29)	−0.2155(42)		117	$F_{23}^{(3)}$	2.69(11)		10^{-2}
112	$F_3^{(3)}$	−0.313(12)	0.1858(22)		118	$F_{33}^{(3)}$	4.14(13)		10^{-2}
113	$F_{11}^{(3)}$	−1.182(27)	0.212(22)	10^{-2}	119	$F_{\ell\ell}^{(3)}$	1.12(43)	2.06(16)	10^{-3}
114	$F_{12}^{(3)}$	0.513(51)	−1.043(27)	10^{-2}	120	$F_J^{(3)}$	−0.95(11)	−1.286(49)	10^{-5}
Parameters of anharmonic interaction matrix element $\langle V_1V_2\ell_2V_3J\|H^{\text{eff}}\|V_1V_2-4\ell_2V_3+1J\rangle$									
121	$F_e^{(4)}$	−0.1477(61)	−0.3418(30)		124	$F_3^{(4)}$	−1.711(97)	3.113(50)	10^{-2}
122	$F_1^{(4)}$	3.884(63)	1.605(60)	10^{-2}	125	$F_J^{(4)}$	0.758(29)	0.510(11)	10^{-5}
123	$F_2^{(4)}$	−0.220(44)	0.388(25)	10^{-2}					
Parameter of anharmonic interaction matrix element $\langle V_1\ V_2\ell_2V_3J\|H^{\text{eff}}\|V_1-2V_2+4\ell_2V_3J\rangle$									
126	$F_e^{(5)}$	2.456(60)	10^{-2}						
Parameters of anharmonic interaction matrix element $\langle V_1V_2\ell_2V_3J\|H^{\text{eff}}\|V_1-3V_2+2\ell_2V_3+1J\rangle$									
127	$F_e^{(7)}$	5.52(43)	10^{-2}	129	$F_3^{(7)}$	4.7(17)	10^{-3}		
128	$F_2^{(7)}$	−16.33(48)	10^{-3}	130	$F_J^{(7)}$	−4.25(15)	10^{-6}		
Parameters of anharmonic interaction matrix element $\langle V_1\ V_2\ell_2V_3J\|H^{\text{eff}}\|V_1V_2-4\ell_2V_3+1J\rangle$									
131	$F_e^{(10)}$	1.05(15)	−1.558(79)	10^{-3}	134	$F_3^{(4)}$	1.60(39)		10^{-4}
132	$F_1^{(10)}$	−3.71(21)		10^{-4}	135	$F_J^{(4)}$	−1.415(85)	0.218(50)	10^{-7}
133	$F_2^{(10)}$	0.391(67)		10^{-4}					
Parameters of anharmonic + ℓ-type matrix elements $\langle V_1V_2\ell_2V_3J\|H^{\text{eff}}\|V_1+\Delta V_1V_2+\Delta V_2\ \ell_2\pm 2V_3+\Delta V_3J\rangle$									
136	F_e^L	0.784(27)	0.7576(98)	10^{-5}	139	F_3^L	1.66(14)		10^{-6}
137	F_1^L	0.454(43)		10^{-6}	140	$F_e^{(3)L}$		−7.01(39)	10^{-6}
138	F_2^L	−0.158(17)		10^{-6}	141	$F_e^{(4)L}$		0.386(56)	10^{-6}

in Ref. [26]. The first set consists of 117 parameters and reproduces the input data with the dimensionless standard deviation $\chi = 1.38$ and RMS of 0.0014 cm^{-1}. It means that such fit practically reaches the experimental accuracy. But there is a primary drawback for this set of parameters: the parameters describing the vibrational dependence of the parameter of anharmonic resonance interaction number 10 are too large with respect to the values required by the perturbation theory. To avoid this inconsistency, we obtained the second set of fitted parameters. This set containing 114 parameters, reproduces the input experimental data with $\chi = 1.46$ and RMS = 0.0015 cm^{-1}. We think that the first set is more preferable for the interpolation calculations and the second is more adequate for the vibrational extrapolation calculations. The RMS deviations for each source of the experimental data are given in Table 4. It is shown that the RMS_RITZ is less than RMS1 or RMS2 for each data source. These values give us a quantitative measurement of the effective Hamiltonian model deviations. In Table 5 the band-by-band statistics of the least-squares fitting is given. For each band we give upper and lower polyad numbers $P1$ and $P2$, HITRAN nomenclature of upper and lower states, maximum J value (J_{max}), number of lines included into the fits N_{lin}, root mean square of the band residuals (RMS) and the mean band residual (MRES), and references in which the bands were reparted. The MRES value gives us an idea about how the band residuals scatter around zero. For a perfectly fitted band MRES should be much smaller than RMS. The effective Hamiltonian parameters together with their standard deviations for fits 1 and 2 are given in Table 6. The residuals for all the lines involved in the fit are given in Supplementary material.

6. Vibration–rotation perturbations

During the fitting of the spectroscopic and effective Hamiltonian parameters, we found several bands of $^{14}N^{15}N^{16}O$ are perturbed. The list of the observed perturbed vibrational states is presented in Table 7. As one can see from this table, there are two kinds of the local perturbations: anharmonic and Coriolis. All anharmonic perturbations come from the anharmonic intrapolyad resonance interactions, which have been included in our polyad model of effective Hamiltonian. The line positions of the respective bands are reproduced with a good accuracy with the help of the set of effective Hamiltonian parameters whereas the band-by-band fitted spectroscopic

Table 7
Observed local perturbations of the vibration-rotation states of $^{14}N^{15}N^{16}O$

State	Perturber	J_{pert}[a]	Interaction type
(716)*e*	(802)	25	Coriolis
(802)	(716)*e*	25	Coriolis
(1116)	(1117)		Anharmonic
(1207)	(1206)	24	Anharmonic
(1208)	(1209)		Anharmonic
(14014)	(1515)*e*	34	Coriolis

[a] Value of the angular momentum quantum number at which the energy level crossing takes place.

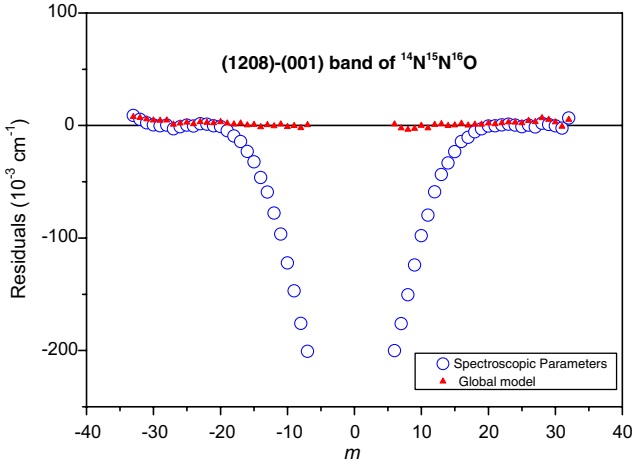

Fig. 4. The residuals between the observed and calculated line positions of the (1208)–(001) band of $^{14}N^{15}N^{16}O$ centered at 6923.4550 cm^{-1}. The calculations have been performed using the set of effective Hamiltonian parameters (Table 6) obtained from global fitting (triangles) and the spectroscopic parameters (Table 3) obtained by the fitting to the observed line positions of this band with high J ($J > 18$) values (open circles). The upper vibrational state (1208) of this band is perturbed by the vibrational state (1209) via intrapolyad anharmonic resonance interactions.

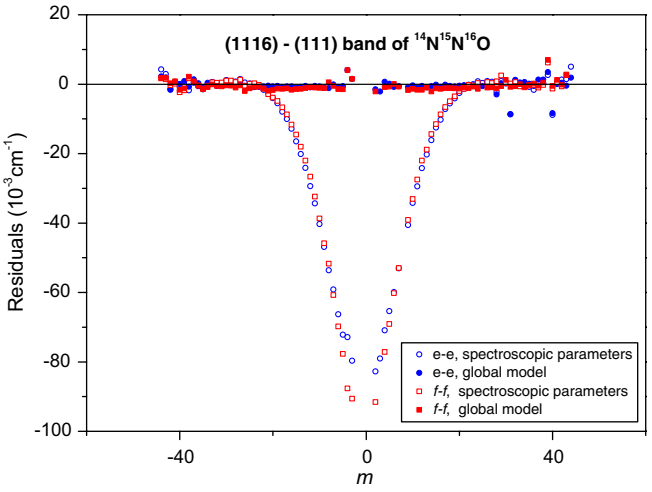

Fig. 5. The residuals between the observed and calculated line positions of the (1116)–(111) band of $^{14}N^{15}N^{16}O$ centered at 5794.7732 cm^{-1}. The calculations have been performed using the set of effective Hamiltonian parameters (Table 6) obtained from the global fitting (■, ●) and the spectroscopic parameters (Table 3) obtained by the fitting to the observed line positions of this band with high J ($J > 20$) values (□, ○). The upper vibrational state (1116) of this band is perturbed by the vibrational state (1117) via intrapolyad anharmonic resonance interactions.

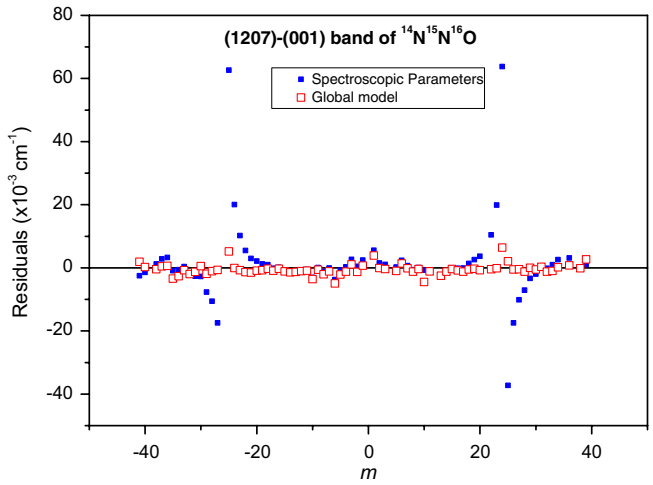

Fig. 6. The residuals between the observed and calculated line positions of the (1207)–(001) band of $^{14}N^{15}N^{16}O$ centered at 6775.2209 cm^{-1}. The calculations have been performed using the set of effective Hamiltonian parameters (Table 6) obtained from the global fitting (□) and the spectroscopic parameters (Table 3) of this band (■). The upper vibrational state (1207) of this band is perturbed by the vibrational state (1206) via intrapolyad anharmonic resonance interactions.

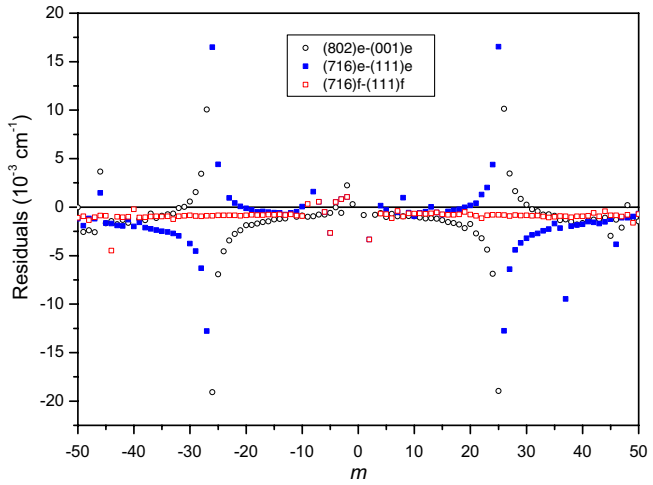

Fig. 7. The residuals between observed and calculated line positions of the (716)-(111) and (802)–(001) bands of $^{14}N^{15}N^{16}O$ centered at 3830.6956 and 4403.7291 cm^{-1} respectively. The calculations have been performed using the set of effective Hamiltonian parameters (Table 6). The upper vibrational states (716) and (802) of these bands are in interpolyad Coriolis resonance interactions.

parameters failed to reproduce these line positions. The examples of the intrapolyad resonance interactions are presented in Figs. 4–6 where the residuals between observed and calculated values of the line positions are presented. Four bands were found to be perturbed via interpolyad Coriolis resonance interactions. These interpolyad resonance interactions have not been taken into account in our effective Hamiltonian model. As a result, the residuals between observed and calculated line positions have resonance behavior near an energy level crossing. For illustration, the residuals for such two bands (716)–(111) and

(802)–(001) are presented in Fig. 7. The upper states of these two bands are in resonance Coriolis interaction. It is clearly shown in this figure that according to the symmetry rules only *e*–*e* subband of the (716)–(111) band is perturbed. If one wants to model these bands with the accuracy close to the experimental uncertainties, it will be necessary to use a non-polyad model of effective Hamiltonian which was discussed in Refs. [10,27–29].

7. Conclusions

The present work considerably extends our knowledge about the high resolution spectra of the $^{14}N^{15}N^{16}O$ isotopolog of nitrous oxide molecule: 80 new bands have been observed for the first time, and the rotational analysis of other 27 bands has been significantly extended and improved. It allowed us to get two sets of effective Hamiltonian parameters which globally describe the line positions of the bands lying in the region 0–8500 cm^{-1} at the accuracy level of 0.001 cm^{-1}. It has been demonstrated that the polyad model of effective Hamiltonian works well for the majority of the observed bands of $^{14}N^{15}N^{16}O$ except four bands perturbed by interpolyad resonance Coriolis interactions which have not been included in the model. The fitted effective Hamiltonian parameters will be used to create spectroscopic N_2O databanks for atmospheric and high-temperature applications.

Acknowledgments

This work is jointly supported by NSFC-China (Grant Nos. 20473079 and 10574124) and RFBR-Russia (Grant No. 06-05-39016), and by the Fok Ying Tong Education Foundation (101013). Dr. F. Qi in NSRL (Hefei) is acknowledged for PIMS mass spectroscopy measurements. We thank B.V. Perevalov, who took part in the initial stage of this research.

Supplementary data

Supplementary data for this article are available on ScienceDirect (www.sciencedirect.com) and as part of the Ohio State University Molecular Spectroscopy Archives (http://msa.lib.ohio-state.edu/jmsa_hp.htm).

References

[1] B.A. Andreev, A.V. Burenin, E.N. Karyakin, A.F. Krupnov, S.M. Shapin, J. Mol. Spectrosc. 62 (1976) 125–148.
[2] I. Morino, M. Fabian, H. Takeo, K.M.T. Yamada, J. Mol. Spectrosc. 185 (1997) 142–146.
[3] B. Drouin, F.W. Maiwald, J. Mol. Spectrosc. 236 (2006) 150–152.
[4] J.M. Krell, R.L. Sams, J. Mol. Spectrosc. 51 (1974) 492–507.
[5] C. Amiot, J. Mol. Spectrosc. 59 (1976) 91–208.
[6] G. Guelachvili, Can. J. Phys. 60 (1982) 1334–1347.
[7] R.A. Toth, J. Opt. Soc. Am. B 3 (1986) 1263–1281.
[8] R.A. Toth, Appl. Opt. 30 (1991) 5289–5315.
[9] R.A. Toth, J. Mol. Spectrosc. 197 (1999) 158–187.
[10] L. Wang, V.I. Perevalov, S.A. Tashkun, B. Gao, L.-Y. Hao, S.-M. Hu, J. Mol. Spectrosc. 237 (2006) 129–136.
[11] H. Herbin, N. Picque, G. Guelachvili, E. Sorokin, I. Sorokina, J. Mol. Spectrosc. 238 (2006) 256–259.
[12] A.-W. Liu, S. Kassi, P. Malara, D. Romanini, V.I. Perevalov, S.A. Tashkun, S.-M. Hu, A. Campargue, J. Mol. Spectrosc. 244 (2007) 33–47.
[13] A.-W. Liu, S. Kassi, V.I. Perevalov, S.A. Tashkun, A. Campargue, J. Mol. Spectrosc. 244 (2007) 48–62.
[14] R.A. Toth, Linelists of water vapor parameters from 500 to 8000 cm^{-1}, see http://mark4sun.jpl.nasa.gov.data/spec/H2O/
[15] J.-L. Teffo, V.I. Perevalov, O.M. Lyulin, J. Mol. Spectrosc. 168 (1994) 390–403.
[16] V.I. Perevalov, S.A. Tashkun, J.-L. Teffo, Sixteenth Colloquium on High Resolution Molecular Spectroscopy, Dijon (France). 6-10 Sept. 1999, Poster D2, pp. 103.
[17] A.V. Vlasova, B.V. Perevalov, S.A. Tashkun, V.I. Perevalov, Fifteenth Symposium on High Resolution Molecular Spectroscopy, Nizhnii Novgorod (Russia). 18-21 July 2006, Poster D20, pp. 86.
[18] G. Amat, H.H. Nielsen, J. Mol. Spectrosc. 2 (1958) 152–162.
[19] G. Amat, H.H. Nielsen, G. Tarrago, Rotation-vibration of polyatomic molecules, Dekker, New York, 1971.
[20] J. Pliva, J. Mol. Spectrosc. 27 (1968) 461–488.
[21] J.-L. Teffo, A. Chedin, J. Mol. Spectrosc. 135 (1989) 389–409.
[22] R.A. Toth, http://mark4sun.jpl.nasa.gov.
[23] S.A. Tashkun, V.I. Perevalov, J.-L. Teffo, M. Lecoutre, T.R. Huet, A. Campargue, D. Bailly, M.P. Esplin, J. Mol. Spectrosc. 200 (2000) 162–176.
[24] S.A. Tashkun, Vl.G. Tyuterev, in: A.I. Nadezhdinskii, Yu.N. Ponomarev, L.N. Sinitsa (Eds.), Proceedings of the 11th Symposium and School on High-Resolution Molecular Spectroscopy, SPIE Proceedings, vol. 2205, 1993, pp. 188–191.
[25] F.L. Chan, K.M. Lau, C.L. Li, H.M. Mok, D.J. Newman, N. Betty, Computers in Physics 3 (1989) 47–51.
[26] J.-L. Teffo, A. Chédin, J. Mol. Spectrosc. 135 (1989) 89–409.
[27] A. Campargue, G. Weirauch, S. Tashkun, V. Perevalov, J.-L. Teffo, J. Mol. Spectrosc. 209 (2001) 198–206.
[28] Y. Ding, V.I. Perevalov, S.A. Tashkun, J.-L. Teffo, S.-M. Hu, E. Bertseva, A. Campargue, J. Mol. Spectrosc. 220 (2003) 80–86.
[29] E. Bertseva, A. Campargue, V.I. Perevalov, S.A. Tashkun, J. Mol. Spectrosc. 226 (2004) 196–200.